

AN ABSTRACT OF THE THESIS OF

Sumantra Bose for the degree of Master of Science in Industrial Engineering
presented on September 25, 2008.

Title: An Internal Convective Heating Technique for Diffusion Bonding Highly Parallel
Microchannel Architectures

Abstract approved:

Brian K. Paul

Diffusion bonding cycle times can be a large cost factor in the production of metal microchannel devices. The challenge is to significantly minimize this cost by reducing the bonding cycle time through rapid and uniform heating and cooling within the bonding process. Heating rates in diffusion bonding processes are typically limited by the need to minimize internal thermal gradients during bonding. A novel method is described which takes advantage of the internal flow passages within microchannel devices for convective heat transfer during the bonding process. The internal convective heating (ICH) technique makes use of heated inert gas to provide the microchannel assembly with rapid and uniform heat input. The first paper in this thesis manuscript investigates the feasibility of the ICH method by studying leakage rates and thermal requirements within the process.

The second paper provides results and a statistical analysis demonstrating that the ICH technique is feasible and capable of shorter bonding cycle times than traditional vacuum hot press methods. Results suggest that this may be due to smaller thermal gradients within microchannel devices during the ICH bonding cycle. Appendices are provided at the end of this manuscript providing the raw data to support these findings.

An Internal Convective Heating Technique for Diffusion Bonding Highly Parallel
Microchannel Architectures

by

Sumantra Bose

A THESIS

submitted to

Oregon State University

in partial fulfillment of
the requirements for the
degree of

Master of Science

Presented September 25, 2008
Commencement June 2009

Master of Science thesis of Sumantra Bose presented on September 25, 2008.

APPROVED:

Major Professor representing Industrial Engineering

Head of the School of Mechanical, Industrial & Manufacturing Engineering

Dean of the Graduate School

I understand that my thesis will become part of the permanent collection of Oregon State University libraries. My signature below authorizes release of my thesis to any reader upon request.

Sumantra Bose, Author

ACKNOWLEDGEMENTS

I would like to express my sincere thanks to my advisor, Dr. Brian K. Paul, for giving me the opportunity to pursue my graduate studies at Oregon State University under his valuable guidance. I had the wonderful experience of working with him on one of the most upcoming technologies in modern day engineering.

My appreciation is extended to Dr. Daniel R. Palo (PNNL), who had provided me with all the support and guidance that was needed throughout my tenure at the university. I would also like to greatly appreciate the efforts of Benjamin Roberts (PNNL), for providing immense help in the setup of my experiments.

Specially, I would like to thank Dr. Sundar V. Atre, for serving as my minor professor in Manufacturing Engineering and guiding me through some of my graduate coursework.

My appreciation is extended to Mr. Steve Etringer, for his valuable machining work and assistance in my research activities at Oregon State University. I would also like to thank Todd Miller and Jack Rundel, who were always supportive of my experimental work at ONAMI (B11), along with providing valuable tips and insights.

I am also especially thankful for the encouragement and assistance of all my fellow graduate students who made the experience of studying abroad unique and enjoyable.

Most of all, I would like to express gratitude and love to my parents, family, and friends, for supporting me throughout and helping me overcome the hurdles along the way.

TABLE OF CONTENTS

<u>Chapter</u>	<u>Page</u>
Chapter 1 - Introduction	1
Chapter 2 - Leakage rates and thermal requirements for the diffusion bonding of microchannel arrays via internal convective heating	4
Chapter 3 - An internal convective heating system for diffusion bonding highly parallel microchannel architectures	21
1. Introduction	21
2. Experimental approach.....	25
2.1 Thermal load and distribution.....	27
2.2 Platen assembly design.....	30
2.2.1 Microchannel Test Article.....	30
2.2.2 Platen Assembly.....	31
2.2.3 Leakage Tests.....	31
2.2.4 Final ICH Test Setup.....	34
2.3 Experimental design.....	36
2.4 Experimental Protocol.....	37
2.4.1 Pre bonding protocol.....	37
2.4.2 In process Protocol.....	38
2.4.3 Post bonding protocol.....	39
3. Results and discussion.....	41

TABLE OF CONTENTS (Continued)

	<u>Page</u>
4. Conclusions and Future work.....	46
Chapter 4 - Summary.....	48
Appendices.....	50
Bibliography.....	94

LIST OF FIGURES

<u>Figure</u>		<u>Page</u>
1.1	Classification of microfluidic devices: (left) analytical microfluidics also known as micro total analysis systems; and (right) arrayed microfluidics also known as micro energy and chemical systems.....	5
2.1	Comparison of cycle time on VHP and ICH.....	7
2.2	Simplified schematic of an internal convective heating setup	8
2.3	Assembly of platens and laminae.....	9
2.4	Bonded platens with shims	10
2.5	Schematic of leakage test setup	11
2.6	Leakage vs Clamping pressure with varying back pressure...	13
2.7	Leakage vs clamping pressure with boron nitride coating.....	14
2.8	Exploded view of INC 625 heat exchanger.....	15
2.9	Gas temperature as a function of distance in heat exchanger....	19
2.10	Temperature distribution of argon in the channel.....	19
3.1	Schematic of microlamination approach.....	22
3. 2	Progression of void elimination within a typical diffusion bonding cycle.....	23
3.3	Cycle time comparison of diffusion bonding cycles in a vacuum hot press (VHP) showing slow ramp rates and using internal convective heating showing fast ramp rates.....	24
3.4	Conceptual ICH diagram with thermocouple placements and PID loop.....	25
3.5	The effect of mass flow rate on heating time assuming a fixture mass of 400 grams and an inlet temperature of 950 °C.....	28

LIST OF FIGURES (Continued)

<u>Figure</u>	<u>Page</u>
3.6. Thermal modeling results on ICH using COMSOL.....	29
3.7. Test article architecture.....	30
3.8. Platen assembly design with test article.....	31
3.9. Leak rate vs Clamping pressure with varying back pressures...	32
3.10. Percentage leak rate versus clamping pressure with/without diffusion barrier.....	34
3.11. Internal convective heating test loop.....	35
3.12. VHP sample produced with typically low heating and cooling rates showing low void fraction and well defined microchannel geometries...	37
3.13. Flow shim of microchannel test article.....	39
3.14. Sectional views of microchannel test article.....	40
3.15. Metallography results for test articles produced using (top) ICH and (bottom) VHP methods. Channel height for the test article design is 375 μm	41
3.16. Warpage in ICH samples.....	42
3.17. Warpage in VHP samples.....	42
3.18. Cross sections of ICH(left) and VHP (right) using aqua regia etch..	44
3.19. 3D representation of average % void fractions in ICH (left) and VHP (right) in different regions.....	44
3.20. Data generated by thermocouples in the ICH test loop.....	45
3.21. 2D plot showing average void fractions in ICH samples	45
3.22. Thermocouple data from VHP final conditions.....	46

LIST OF TABLES

<u>Table</u>	<u>Page</u>
Table 1. Leakage test variables	10
Table 2. Heat exchanger channel dimensions.....	15
Table 3. Thermodynamic properties of argon.....	16
Table 4. Coefficient of heat transfer and mass flow rates.....	18

LIST OF APPENDICES

<u>Appendix</u>	<u>Page</u>
A: Literature review	49
B: Test Setup	57
C: Results and Data collection	77

Dedicated to
My dear grandfather,
Mr. Jyotirmoy Mazumdar

1. INTRODUCTION

The field of microfluidics has attracted increasing interest because of the ability to miniaturize many macro-scale chemical and fluidic operations leading to distributed and portable applications with precise chemical process control. This miniaturization is made possible by the high surface area to volume ratios available within microchannel structures. Fluids processed within microchannel structures have short diffusional distances leading to faster heat and mass transfer rates.

As shown in Figure 1.1¹, microfluidic devices can mainly be classified into two groups: analytical microfluidic devices, also known as micro total analysis systems (μ -

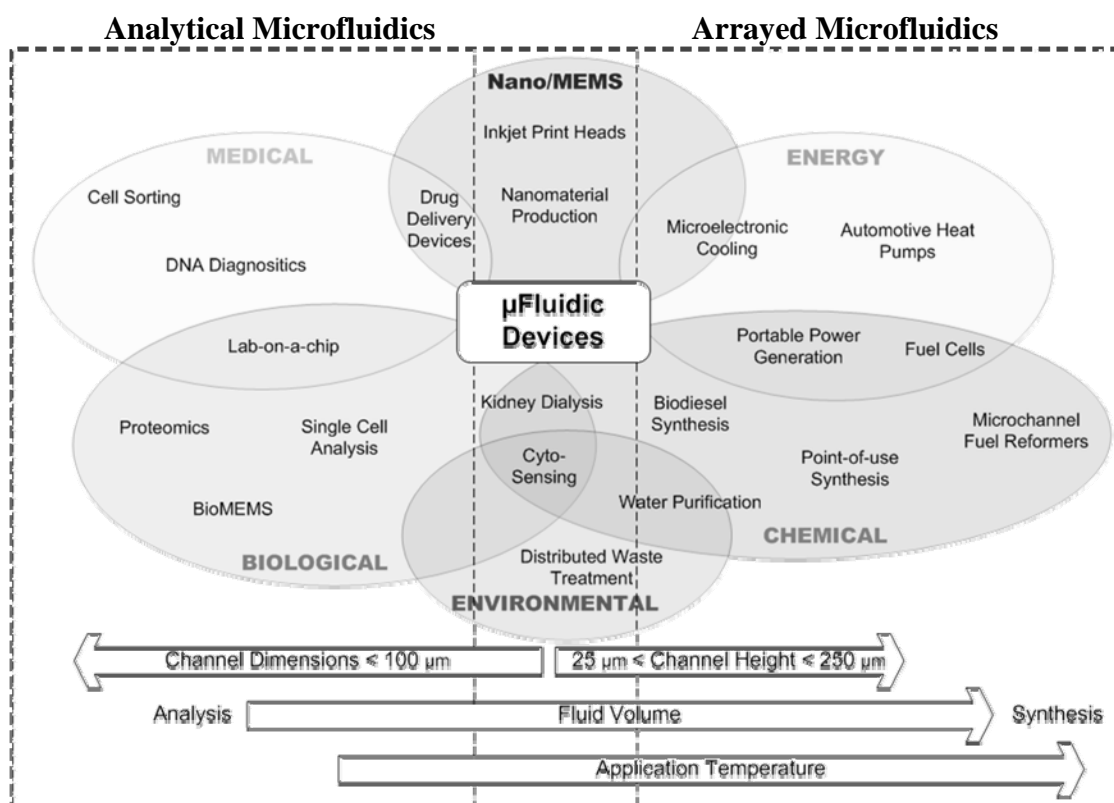


Figure 1.1. Classification of microfluidic devices: (left) analytical microfluidics also known as micro total analysis systems; and (right) arrayed microfluidics also known as micro energy and chemical systems.

TAS), and arrayed microfluidic devices, referred to as micro energy and chemical systems (MECS). These two major categories have significant differences in their function and in the materials and fabrication technologies used to implement them. The purpose of analytical devices is to quickly assay small samples of fluids to determine composition and other information about the sample. Continued advances in analytical microfluidics are fueling radical innovations in medicine. These applications tend to operate near room temperature such that device materials include many polymers. Further, analytical devices require higher levels of control and sensing which is compatible with many polymer, glass and silicon architectures. These materials are all congruent with existing microelectronics and MEMS fabrication technologies.

Arrayed microchannel devices are typically produced through a lamination process where thin metal shims are cut, patterned, and possibly coated. The prepared shims are then stacked in an appropriate sequence and bonded by diffusion bonding or diffusion brazing. Regardless of the bonding technique used, the assembly is usually held under pressure in an inert or reducing atmosphere and heated by radiation and/or free convection in a furnace or hot press. A recent study by OSU has shown that bonding cycle time is one of the largest cost factors in the short-run production of arrayed microchannel components, representing between 40 and 87% of the fabrication cost. Other studies have shown that thermal gradients caused by fast heating and cooling rates at the beginning and end of the diffusion bonding cycle is a major source of microchannel warpage. This research is primarily aimed at significantly reducing the bonding cycle time and associated warpage associated with rapid and uniform heating and cooling of arrayed microchannel components during the bonding process.

In the following manuscript, two papers are used to describe a unique internal convective heating (ICH) technique for utilizing the internal flow passages of arrayed microchannel (ArM) devices to deliver thermal energy convectively to the internal surfaces of ArM devices during diffusion bonding. The first paper investigates the feasibility of the ICH method by studying leakage rates and heat exchanger requirements within the process. The second paper documents the primary results and conclusions obtained in this research. Findings show that the novel ICH technique is feasible with advantages over existing vacuum hot press methods of diffusion bonding. The research goes on to define some of the practical constraints associated with this method. Appendices are provided at the end of this manuscript to support these findings by providing additional results. The next chapter investigates the feasibility of the ICH method by studying leakage rates and thermal requirements within the process

2. LEAKAGE RATES AND THERMAL REQUIREMENTS FOR THE DIFFUSION BONDING OF MICROCHANNEL ARRAYS VIA INTERNAL CONVECTIVE HEATING

2nd International Conference on Micromanufacturing 2007
Sumantra Bose¹, Daniel R. Palo², Brian K. Paul³

¹Sumantra Bose; Dept. of Industrial Eng., Oregon State University;
e-mail: bosesu@onid.orst.edu

²Daniel R. Palo; Pacific Northwest National Laboratory; e-mail: dpalo@pnl.gov

³Brian K. Paul ; Dept. of Industrial Eng. Oregon State University;
e-mail: brian.paul@oregonstate.edu

Abstract

Diffusion bonding cycle times can be a large cost factor in the production of metal microchannel devices. The challenge is to significantly minimize this cost by reducing the bonding cycle time through rapid and uniform heating and cooling within the bonding process. Heating rates in diffusion bonding processes are typically limited by the need to minimize internal thermal gradients during bonding. A novel method is described which takes advantage of the internal flow passages within microchannel devices for convective heat transfer during the bonding process. The internal convective heating (ICH) technique makes use of heated inert gas to provide the microchannel assembly with rapid and uniform heat input. This paper investigates the feasibility of the ICH method by studying leakage rates and thermal requirements within the process.

Introduction

Microlamination is a process architecture commonly used to fabricate monolithic, multi-layered bulk microfluidic devices having complex internal cavities consisting of highly parallel arrays of microchannels^{2,3}. Microchannels are good for increasing surface to volume ratios critical for reducing diffusional distances in heat and mass transfer. Arrays are necessary to increase flow rates and throughput.

Microlamination involves the patterning and bonding of thin layers of material, called laminae. Laminae can be designed to implement a host of functions (e.g., mixing, reaction, heat transfer) within a microchannel format. For instance, deposition of catalytic materials on laminae can be used in the fabrication of microreactors to conduct heterogeneous catalysts⁴. Patterning of the shims can be accomplished in large quantities at low cost per shim by using photochemical machining or stamping processes. After patterning of the individual fluidic layers, diffusion bonding is often used to consolidate a stack of laminae. As implied above, stacking of laminae permits scale-up of microchannel functionality. A critical step during the bonding of the patterned layers is the proper alignment and registration of the layers relative to each other. Commonly, alignment of the layers is achieved with pins and precise pinholes in the layers. During diffusion bonding, laminae are heated up to the bonding temperature under an applied bonding pressure typically within a vacuum hot press (VHP). These pressure and temperature conditions are held constant for a period of time necessary to convert the layers into a monolithic device via solid state diffusion. Insufficient bonding conditions can lead to poor bonding and leakage⁵ while extreme bonding conditions may lead to deformed or collapsed channel features.

Researchers have developed and fabricated numerous microchannel-based reactors, heat exchangers, and separators within the context of basic and applied research projects, where unit cost is unimportant relative to other factors such as performance, weight, and size. As microtechnology has progressed, the need and desire for lower-cost manufacturing techniques have come to the forefront in making microtechnology acceptable to clients and potential customers. A recent study by OSU has shown that bonding cycle time can be one of the largest cost factors in the production of bonded devices, representing between 40% and 87% of the fabrication cost. The report also found that capital cost and heating and cooling rates were very strong drivers of cost performance.

Internal Convective Heating

Heating and cooling rates in furnace bonding processes are usually limited by the need to minimize thermal gradients within the assembly (shim stack) being bonded. Rapid heating of the assembly by external heating and intra-assembly conduction leads to significant thermal gradients within the assembly, which can cause shim deformation, channel obstruction, and residual mechanical stresses within the finished part. These mechanical considerations limit the heating/cooling rate to about 5 °C per minute depending upon the size of the hot press and the size of the device being bonded. For bonding cycles that require temperatures around 1000 °C, this represents a very long duration during ramp-up. This problem is further compounded as the size of the bonded device increases. Since microchannel devices are already equipped with internal flow channels, we have proposed to utilize these channels for heat transfer in the rapid and

uniform heating and cooling of the laminated assembly during diffusion bonding. It is expected that heated fluid (inert gas, reducing gas, or other) can be forced through the prepared shim stack to provide heat for bonding.

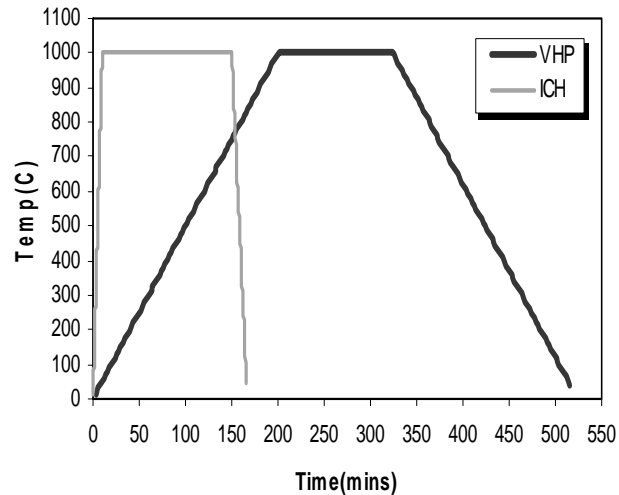


Figure 2.1. Comparison of cycle time on VHP and ICH.

This internal convective heating (ICH) bonding technique can provide the assembly with rapid heat input while minimizing thermal gradients within the assembly.

As compared to traditional VHP methods, it is conceivable that the ICH method could bring the system up to the bonding temperature in less than 10 minutes depending upon device and process constraints such as thermal gradients allowable within the stack. Heating and cooling times on this order could lead to cycle time reduction of more than 50% as shown in Figure 2.1. In Figure 2.1, the constant temperature region is where the bonding pressure is applied and diffusion bonding takes place.

One of the challenges of the ICH approach is the potential for gas leakage during bonding. Too high of a leakage rate could factor into the economics of the process. Another challenge is the design of a thermal system capable of delivering the necessary heat at the proper flow rates for controlling the process. The objective of this paper is to analyze leakage rates and thermal requirements for the ICH process.

Process Design

A process design was developed for a typical 25 x 25 mm microchannel test article made from stainless steel 316L. The basic design of the shim assembly consists of two stainless steel 316L flow shims (1.0"x1.0"x.015") sandwiched between two end plates and a middle plate. The end plates provide manifolding to the flow shims and the middle plate keeps the two flow shim fluid streams separate.

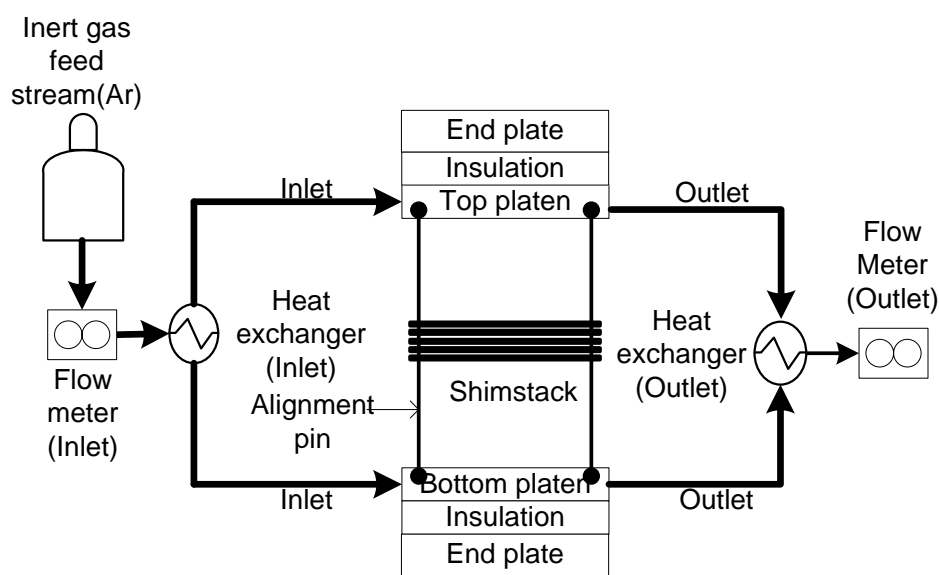


Figure 2.2. Simplified schematic of an internal convective heating setup.

Figure 2.2 shows a simplified schematic of the ICH test stand designed to support representative bonding experiments. As shown in the system schematic, a heat exchanger is used at the inlet to provide heat to the inert gas being used as the heat transfer fluid. Argon is used as the heat transfer fluid because of its inert nature and low cost. A platen assembly was required to couple the gas stream into the pressure subsystem (Figure 2.3).

For proof-of-principle testing, it was decided that bonding pressure could be supplied by the hydraulic subsystem of a VHP. This requires the ICH test stand to be set up adjacent to a VHP and operate within the work envelope of the system. In the current test stand, the work envelope is constrained to a maximum of a 75 mm

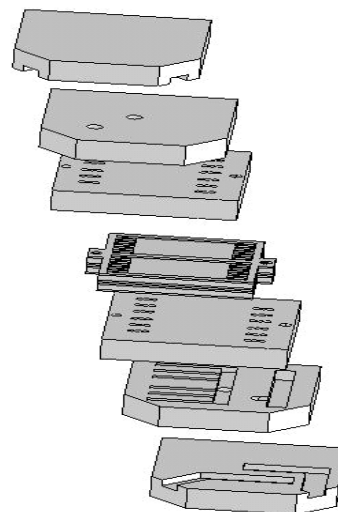


Figure 2.3. Assembly of platens and laminae.

diameter. During warm-up, the purpose of the clamping mechanism is to provide enough pressure to keep the heat exchange gas from leaking out between the shims. During the bonding period, the pressure is required for solid state diffusion across faying surfaces. Typical pressures of 1000-1200 psi are required during the bonding step.

Both the heat exchanger assembly and the shim stack require thermal isolation for proper operation, efficiency, and safety. Zircal-95 was chosen as the insulation material for the platen assembly. An enclosure around the shim stack is also envisioned to provide a safety shield. Flow controllers, thermocouples, and flow meters are designed to provide feedback for the process. A computer-based data acquisition system will be used to control the process.

Leakage Study

The objective of the leakage study was to investigate the amount of gas leakage resulting from an ICH setup. The leakage from between the laminae and platens was studied as a function of applied pressure to the stack and surface conditions of the

Table 1. Leakage test variables

Independent Variables	Dependent Variables
Gas flow rate, Clamping pressure, Surface conditions: flatness, roughness, burr height	Volumetric leakage

laminae.

Leakage tests were performed to determine the clamping pressure required to acceptably minimize leakage of convective gases from the bonding assembly. It was hoped that clamping pressures would be on the same order of magnitude as bonding pressure or lower. The temperature of the gas in the assembly will be near or at 1000°C , which is the required temperature for the diffusion bonding of stainless steel. Thus the minimization of leakage is also critical to maximize safety. Process conditions to be investigated by the study are shown in Table 1.

Experimental Setup

Figure 2.4 shows a three dimensional model of the platen assembly designed for diffusion bonding the set of stacked laminae. Both the top and bottom platens consist of three AISI stainless steel 321 plates (1.2"x1.2"x0.2") with flow paths machined on the surface of each plate to allow for the passage

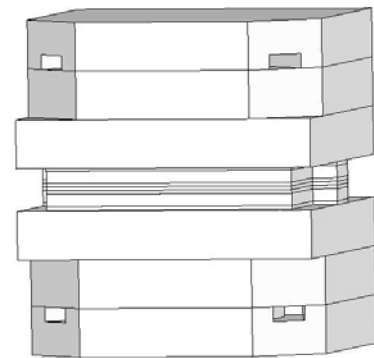


Figure 2.4. Bonded platens with shims

of argon gas. Each set of platens was diffusion bonded in a VHP at a pressure of 1000 psi and a temperature of 1000°C for 3 hours. The platens consist of an inlet and an outlet slot allowing for the entry and exit of argon gas. Stainless steel tubing was TIG welded onto the inlet and outlet slots of each platen. Holes are provided on the platens for pin alignment of the laminated shims.

Before stacking, the shims were cleaned in a solution of Citranox and water. Grease is removed by acetone followed by ethanol and de-ionized water for removal of residues. The set of cleaned laminae were then assembled and aligned with the slots provided on the bonded platen assembly using 1/16" diameter alignment pins. Figure 2.4 shows the shim assembly stacked in between the two platens, ready to be leak tested.

A mass flow controller and a flow meter were connected to the inlet of the compressed air loop at close proximity to the vacuum hot press. A flow meter and a pressure gauge were connected to the outlet stream of the platen assembly. The purpose of the pressure gauge was to measure and vary the back pressure at the outlet of the flow loop. Finally,

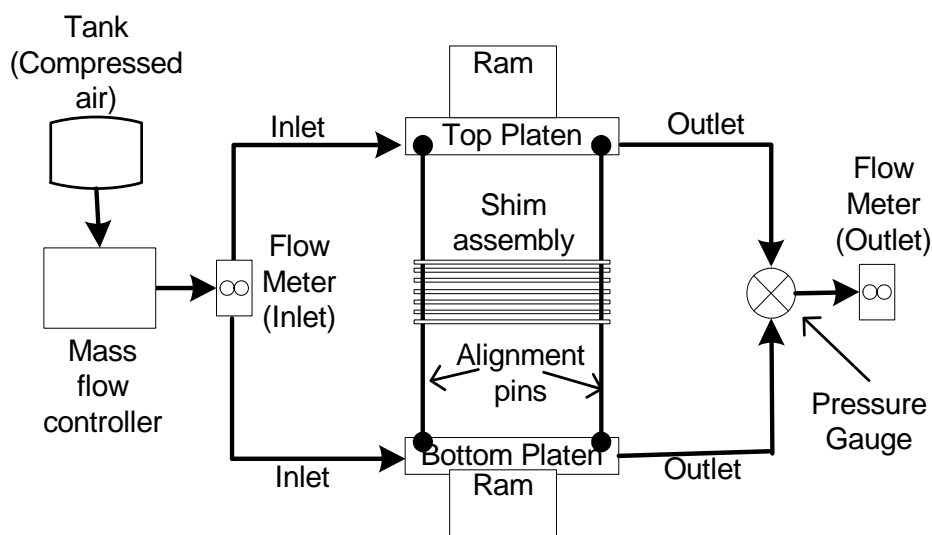


Figure 2.5. Schematic of leakage test setup

the assembly was clamped between the hydraulic rams of the vacuum hot press. The schematic representation of the setup used in performing the leak tests is shown in Figure 2.5.

As a preliminary leak test, the platens were clamped together with a 'C-clamp'. The assembly was immersed in a beaker containing water, and pressure was applied to check for bubbles. There was no bubble formation within the platens up to a pressure of 35 psi, indicating no leakage from the part.

Experimental Results

The platen assembly was clamped in between the rams of the vacuum hot press and a pressure was kept at a minimum level. The compressed air was turned on and passed through the platen assembly. The clamping pressure was gradually increased using the pressure control panel on the vacuum hot press. Volumetric flow rates at the outlet were measured with increasing clamping pressure using the flowmeter provided at the outlet shown in Figure 2.5. Leakage measurements were carried out by varying back pressures on the outlet ranging from 0 to 20 psi. The flow rate at the inlet was maintained at a constant rate of 21.75 SLPM.

Volumetric leakage was calculated using the following relation: $L = F_{in} - F_{out}$

(1)

Where,

L = Volumetric leakage (SLPM)

F_{in} = Flow rate of the gas at the inlet (SLPM)

F_{out} = Flow rate of the gas at the outlet (SLPM)

Figure 2.6 shows the variation of volumetric leakage with increasing clamping pressure at different back pressures. The leakage was found to be 1.73% at a clamping pressure of 800 psi when there was no back pressure on the outlet line. This is roughly the minimum bonding pressure for the device. Volumetric leakage was found to increase with increasing back pressure.

Back pressure simulates the type of pressure conditions that might be found in larger devices. It was found that 28.2% of the gas leaked when the back pressure was 20 psi at 800 psi clamping

pressure. Given that the pressure drop across the current device was near 2 psi, this is an approximate simulation of a device with 10X the flow path length. At a clamping pressure of 3000 psi and a backpressure of 20 psi, percent leakage was

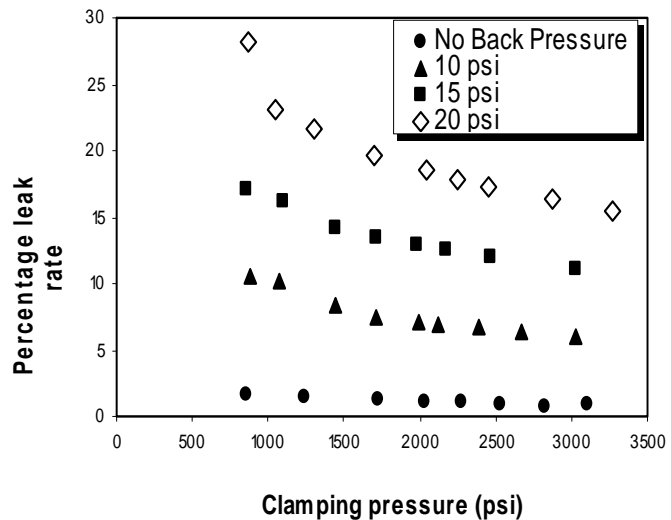


Figure 2.6. Leakage vs Clamping pressure with varying back pressure

found to be approximately 15%. This would be near the upper end of the bonding pressure.

One goal with regard to leakage tests was to analyze the effect of diffusion barriers on leakage. Diffusion barriers are applied to platens to keep the laminae from bonding to the platens. Tests were performed by spray coating a layer of boron nitride particles onto platens prior to running tests. As shown in Figure 2.7, the leakage increased by about 2% with the use of the barrier coating using a back pressure of 10 psi. This is not a significant leak rate increase.

Together, these results suggest that for small devices, the rate of Argon loss due to leakage will not become an

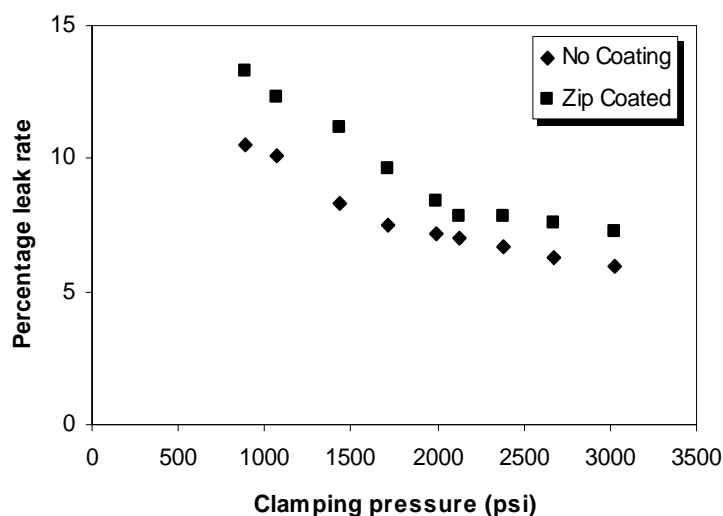


Figure 2.7. Leakage vs clamping pressure with boron nitride coating.

economical barrier. This is particularly so in light of the fact that final implementation of this method will probably be done in concert with a furnace to simultaneously heat the exterior of the device. Therefore, the gas would only be needed for short bursts at the start and finish of the bonding cycle and gas losses would only be incurred at the start.

Table 2. Heat exchanger channel dimensions

Height	Width	Length	Aspect ratio ($\alpha^* = b/a$)
0.003 m	0.025 m	0.590 m	0.120

Thermal analysis of the inlet heat exchanger

The material used for the inlet heat exchanger is Inconel (INC) 625 which is an excellent general

purpose material for high strength applications at elevated temperatures in oxygen atmospheres. An exploded view of the heat exchanger is shown in Figure 2.8. The overall dimensions of the heat exchanger are shown in Table 2. As shown, the INC 625 heat exchanger at the inlet consists of a centre block, a top and a bottom plate and some additional Inconel tubing. The centre block has dimensions of 8.5" x 4.5" x 1.0". Channels are machined on either side of the centre block to allow for the passage of argon gas from two inlets to two outlets. In the middle of the block are three 0.75" diameter through holes for placing nichrome heaters. The heaters are each capable of transferring up to 1000 watts of thermal power at 1400K. The channels on the centre block are covered at

the top and bottom by two INC 625 plates (8.5" x 4.5" x 0.125"). The two inlets and two outlets of the heat exchanger are connected to tube fittings.

The approach to heat exchanger design taken here is similar to that in literature⁶. An estimate of the thermal requirements for the ICH

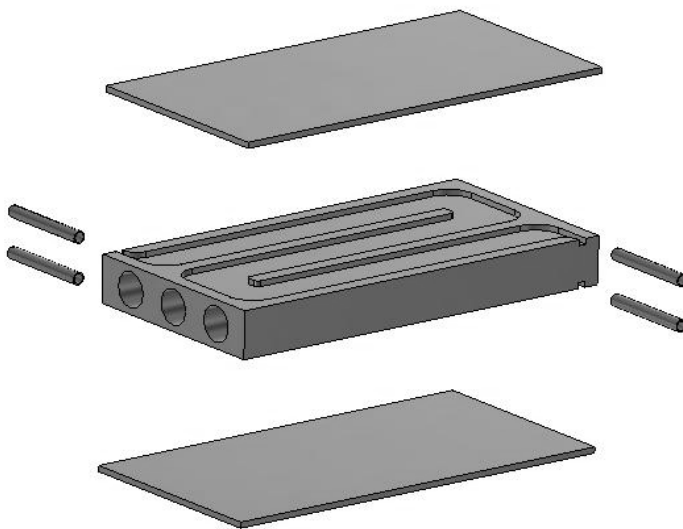


Figure 2.8. Exploded view of INC 625 heat exchanger

system can be made by considering the enthalpy of the thermal mass in the system and making assumptions about heat losses. In our model, we are assuming that heat transfer to the gas occurs from only one wall. This wall is held at a constant temperature of 1200K. The constant temperature boundary condition is present when the duct has a constant wall temperature in both the circumferential and the axial directions.

In fluid mechanics, the Reynolds number is the ratio of inertial forces to viscous forces and consequently it quantifies the relative importance of these two types of forces for given flow conditions⁷. Thus, it is used to identify different flow regimes, such as laminar or turbulent flow.

$$Re = (u \cdot D_h) / \nu \quad (2)$$

Where,

$u \sim$ average velocity of the gas

<i>Table 3. Thermodynamic properties of argon</i>			
Temperature, K	298	748	1200
Molecular weight (MW), kg/mol	0.039	0.039	0.039
Density (ρ), kg/m ³	1.633	1.024	0.526
Specific heat (C_p), kJ/kg.K	0.520	0.520	0.520
Viscosity (η), kg/m.sec (10 ⁵)	2.26	4.44	5.99
Thermal conductivity (k), W/m.K	0.01769	0.0351	0.048

$\nu \sim$ kinematic fluid viscosity, $\nu = \eta / \rho$

η , ρ are viscosity and density of argon gas respectively

and,

$$u = Q / A \quad (3)$$

where,

Q is the volumetric flow rate

A is the cross sectional area of channel

$$\begin{aligned} u &= 0.000416 \text{ m}^3/\text{sec} / 0.0000772 \text{ m}^2 \\ &= 5.388 \text{ m/sec} \end{aligned}$$

In this application, the value of the Reynolds number above 300 K lies below 2300 suggesting laminar flow. The thermodynamic properties of argon gas were calculated at different temperatures ranging from 298-1200K⁸. The values of molecular weight, density, specific heat, viscosity and thermal conductivity of argon at 298, 748, and 1200K are provided in Table 3.

In order to design a plate-type heat exchanger capable of meeting these requirements, the mass flow rate and an estimation of the convective heat transfer coefficient is needed.

Coefficient of heat transfer and mass flow rate

The convective heat transfer coefficient for this application can be estimated by^{9,10}:

$$h = Nu_T \cdot k / D_h \quad (2)$$

Where,

$Nu_T \sim$ Nusselt number at constant wall temperature of 925 °C

D_h ~ hydraulic
 diameter
 k ~ thermal
 conductivity of
 argon
 h ~ coefficient
 of heat transfer

<i>Table 4. Coefficient of heat transfer and mass flow rates</i>			
Temperature (Kelvin)	298	748	1200
Heat Transfer Coefficient(W /m ² K)	1.832	3.370	4.702
Mass flow rate(kg/sec)	0.00067	0.00042	0.00021

The Nusselt number for fully developed laminar flow in rectangular ducts with heat transfer through one wall is 0.5322 [7]. The hydraulic diameter is given by

$$D_h = 4ab/(2*(a+b)) \quad (4)$$

where

a and b are channel height and width respectively

$$D_h = 0.00543\text{m}$$

The mass flow rate can be calculated as

$$m = \rho \cdot Q \quad (5)$$

where,

ρ ~ density of argon gas

Q ~ volumetric flow rate

The required volumetric flow rate for incoming argon gas at 1200K has been calculated to be 25 SLPM according to enthalpy requirements and heat losses. Using (4) and (5), the coefficient of heat transfer and mass flow rate was calculated and the values obtained are shown in Table 4.

Thermal Modeling

Given the data above, a computational fluid dynamics thermal model was generated. The purpose of the thermal model was to determine if the surface area of the channel

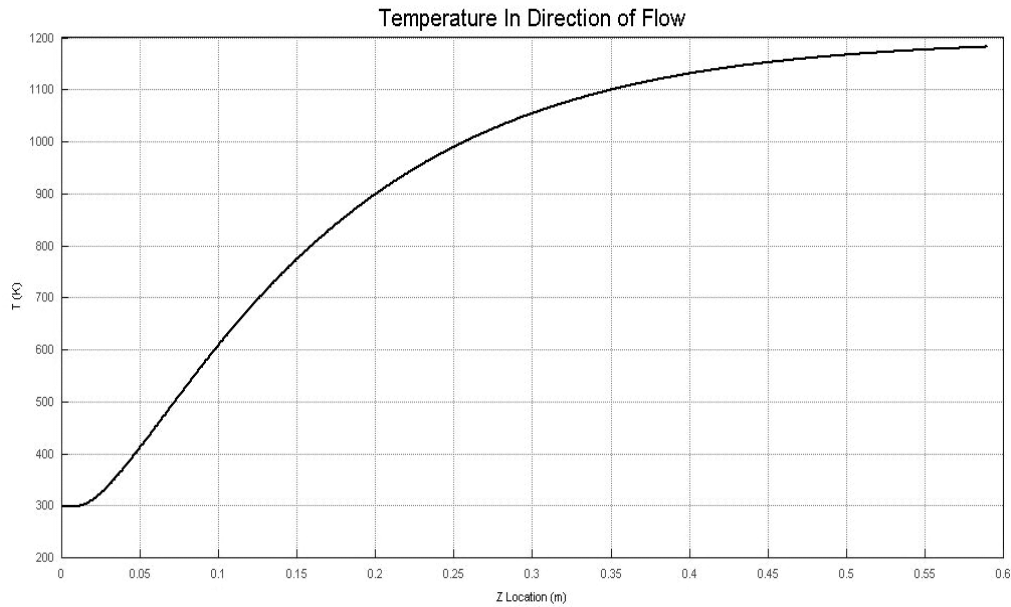


Figure 2.9. Gas temperature as a function of distance in heat exchanger.

would be sufficient to heat the room temperature argon gas to the bonding temperature of the microchannel device. Figures 2.9 and 2.10 show the temperature distribution of argon flowing from the inlet through the channel, which is machined into the centre plate of the heat exchanger. The inlet velocity was set to 5 m/s and the temperature of incoming Argon gas was

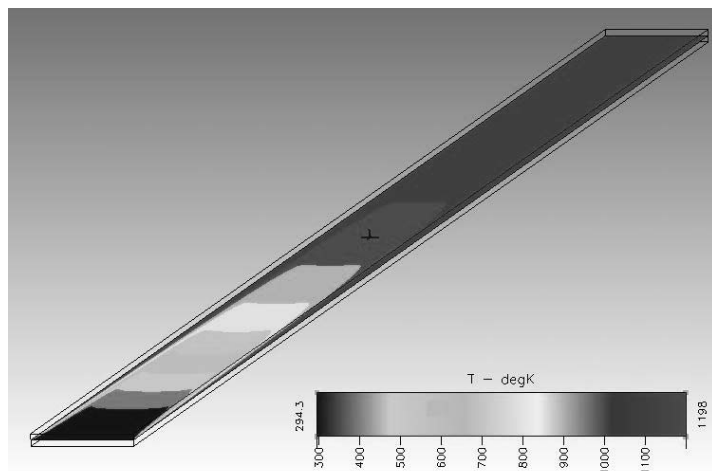


Figure 2.10. Temperature distribution of argon in the channel

set to 300K. Argon gas properties were provided in piece-wise linear form using data for temperatures 298K, 748K, and 1200K. All walls were set to a no slip condition at 1198K.

In Figure 2.9, the axial thermal distribution shows a gradual change in temperature from the inlet towards the outlet. This analysis suggests that the Argon gas was heated to greater 1150 K within a distance approximately equal to 0.5 m from inlet. This analysis was used to validate the dimensions of the heat exchanger. Longer term, a recuperation system to recycle inert gas from the outlet back into the heat exchange device is envisioned.

Summary and future work

Leakage tests have been performed to determine the clamping pressure required to acceptably minimize the leakage of convective gases from the bonding assembly. The low leak rates confirm the feasibility of operating the ICH system for bonding microchannel devices. A plate type heat exchanger has been designed which successfully heats argon to the bonding temperatures required. This heat exchanger will provide the microchannel assembly with rapid heat input.

The heat exchanger is currently being fabricated using conventional machinery in the OSU fabrication facility. Once this heat exchanger has been fabricated, the final test loop will be assembled and operated. Eventually, samples diffusion bonded on the VHP will be compared to those successfully bonded using internal convective heating to evaluate the bond quality of the ICH bonding system for bonding microchannel devices.

3 AN INTERNAL CONVECTIVE HEATING TECHNIQUE FOR DIFFUSION BONDING HIGHLY PARALLEL MICROCHANNEL ARCHITECTURES

S. Bose, B. K. Paul, D. R. Palo

1 INTRODUCTION

The field of microfluidics has attracted increasing interest because of the ability to miniaturize many macro-scale chemical and fluidic operations leading to distributed and portable applications with precise chemical process control. This miniaturization is made possible by the high surface area to volume ratios available within microchannel structures. Fluids processed within microchannel structures have short diffusional distances leading to faster heat and mass transfer rates.

Microfluidic devices mainly can be classified into two groups: analytical microfluidic devices, also known as micro total analysis systems (μ -TAS), and arrayed microfluidic devices, referred to as micro energy and chemical systems (MECS). Continued advances in analytical microfluidics are fueling radical innovations in medicine. Analytical microfluidics assay small samples of fluids near room temperature to determine composition and other information about the sample. These requirements are all congruent with existing MEMS and BioMEMS fabrication technologies.

In contrast, arrayed microfluidic devices are designed to process bulk quantities of fluids through the use of microchannel array¹¹. Potential arrayed microfluidic applications exist in abundance. Residential air conditioning could be made “ductless” through the application of many distributed micro heat pumps. Biodiesel microreactors have the potential to shrink plant size by 100 to 1000 times greatly reducing capital

investments. At-home, portable kidney dialysis will make life more manageable and cost effective for a whole new generation of kidney patients. Many arrayed microfluidic applications require materials capable of withstanding higher temperatures and higher thermal transport. Because they process bulk amounts of fluid, these devices tend to be much larger than analytical devices requiring the use of low-cost, engineering materials.

The vast majority of arrayed microfluidic devices have been produced in metals using a microlamination approach^{12,13}. Microlamination involves the patterning and bonding of thin layers of material, called laminae (see Figure 3.1). Metal laminae can be patterned using

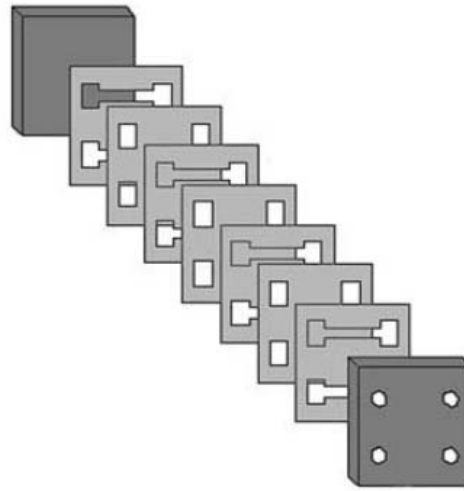


Figure 3.1. Schematic of microlamination approach

photochemical machining or stamping processes. Bonding of metal laminae often involves diffusion bonding. Microchannel arrays have been diffusion bonded in a wide array of metals with features as small as tens of micrometers^{14,15,16,17,18,19}.

Diffusion bonding is a solid state joining process, in which two cleaned and smooth surfaces are pressed together for a certain time at elevated temperatures enabling atoms from each surface to diffuse across the interface forming a metallic bond (Figure 3.2). Diffusion bonding typically is conducted in vacuum to prevent oxidation of the metal shims as the oxide layer may create a diffusion barrier²⁰. To form a satisfactory bond, it is necessary to bring the two metal surfaces into sufficient atomic contact so that

the energy of interaction between their atoms is minimal. Diffusion bonding generally requires surface finishes around $0.4 \mu\text{m Ra}$ to achieve bonding strengths close to that of the parent material²¹. The interatomic forces of attraction begin to be felt at distances between 10^{-4} and 5×10^{-4} micrometers²². Consequently, the application of bonding pressure is needed to bring the surfaces into intimate contact through the plastic deformation of surface asperities. The application of temperature increases the rate of diffusion as well as reduces the strength of surface asperities and surrounding materials. Inadequate bonding conditions can lead to poor bonding and leakage²³ while excessive bonding conditions can lead to severe channel deformation²⁴.

Vacuum hot presses (VHP) are typically used to implement diffusion bonding protocols for arrayed microchannel devices. Typically, stacks of laminae are pressed between hydraulic rams within a vacuum. Thermal energy is delivered from resistive heating elements to the outer surface of the device by radiation. A study performed by OSU researchers has shown that 50 to 80% of the total diffusion bonding cycle time

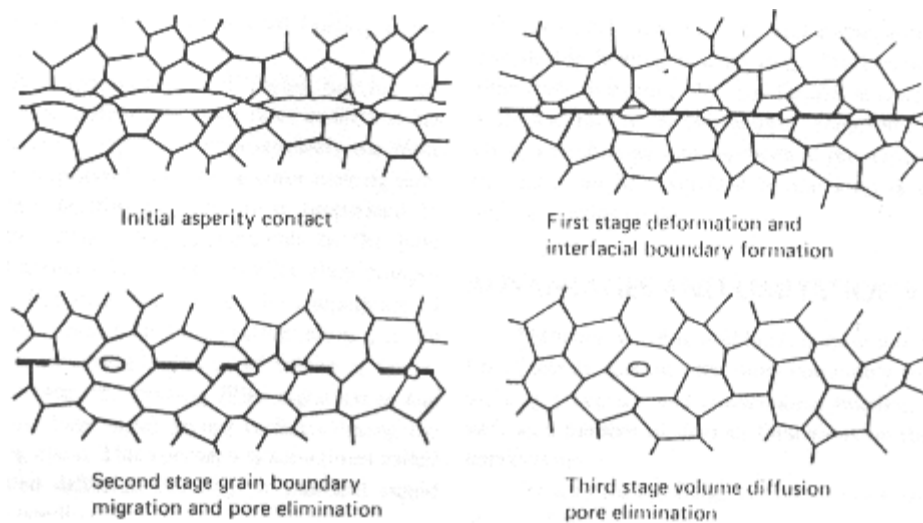


Figure 3.2. Progression of void elimination within a typical diffusion bonding cycle.

within a VHP is due to vacuum pump-down time, heat-up and cool-down time of the VHP (Figure 3.3). Further, there is mounting evidence within industry that aggressive temperature ramp rates cause large thermal gradients within devices being bonded leading to severe channel warpage.

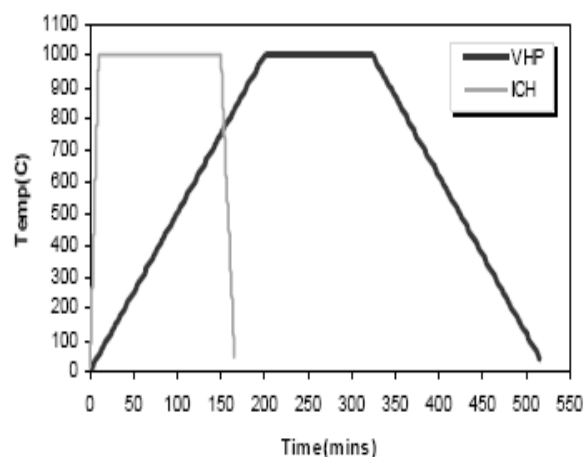


Figure 3.3. Cycle time comparison of diffusion bonding cycles in a vacuum hot press (VHP) showing slow ramp rates and using internal convective heating showing fast ramp rates.

In this investigation, we develop an internal convective heating (ICH) method for the diffusion bonding of metal microchannel laminae by taking advantage of the internal fluid flow pathways within arrayed microfluidic devices to deliver thermal energy convectively to the internal surfaces of the device. It is expected that this method will permit faster processing times than traditional VHP methods of diffusion bonding by permitting faster temperature ramp rates within the diffusion bonding cycle. In addition, it is expected that the ICH method will provide a means to investigate the presence of thermal warpage mechanisms.

2 EXPERIMENTAL APPROACH

Figure 3.4 is a conceptual diagram of the experimental test stand constructed to support the internal convective heating (ICH) of arrayed microfluidic devices during diffusion bonding. Considerations in the design of this setup included thermal and bonding pressure delivery in addition to thermal isolation. High purity (99.99%) argon gas was used as the medium for thermal delivery. An Inconel 625 heat exchanger was designed and fabricated to transfer heat to the argon gas stream for delivery to the stack of laminae to be diffusion bonded. Design of the heat exchanger has been explained elsewhere²⁵. Hot gas flows from the heat exchanger into the platen assembly with the test article and out to a large air handling system. Thermocouples were placed, as shown in numbers one through seven in Figure 3.4 below, to provide temperature feedback for the process. Specific locations included in one of the outlets of the heat exchanger (seven), in the inlets (one and four) and outlets (three and six) of the platen assembly and adjacent

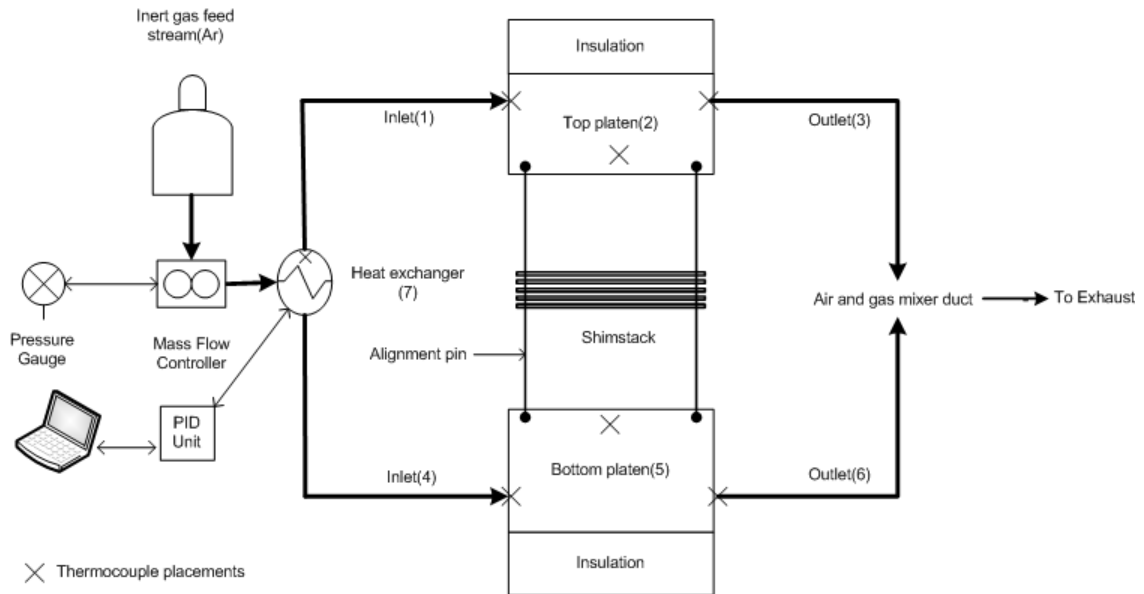


Figure 3.4. Conceptual ICH diagram with thermocouple placements and PID loop

to the surface of the top (two) and bottom (four) platens. Temperature of the inlet gas was monitored using thermocouples one and four connected to data acquisition software. Gas flow was set manually using a mass flow controller with mass flow meters for monitoring. Before the entire process was run, the system was checked for leakage. This was done by checking the gas pressures at the inlet and outlet, and was found to be the same. This ensured that the mass flow rates at the upper and lower loops are equal. A pressure was included in the system to have an estimate of the back pressures in the flow loop.

The function of the bonding pressure delivery system was to provide enough pressure during heat-up to keep the heat transfer gas from leaking out between the shims and to provide enough pressure during the dwell period to result in a strong bond between the shims. Bonding pressure was supplied by a hydraulic ram through upper and lower platens. Platens were adapted to allow for gas flow into and out of the lamina stack. Platens were made from 321 stainless steel to withstand the temperatures and pressures required for the bonding process.

The high temperature portions of the thermal delivery system required thermal insulation and enclosure for proper operation, efficiency, and safety. To thermally isolate the ICH system from the hydraulic press, thick ceramic insulation plates (Zircal-95) were placed between the platens and the hydraulic ram. Fiber insulation (K-wool) was used to further isolate high temperature sections from the ambient. A physical barrier was placed around the shim stack for safety. A computer-based data acquisition system (Omega OMB-DAQ-54) was used to control the temperature of the inlet gas and to monitor the temperature, flow and pressure of the gas within the system.

2.1 THERMAL LOAD AND DISTRIBUTION

Before proceeding with experiments, efforts were made to determine the thermal load and conditions necessary to provide the thermal distribution required for diffusion bonding via internal convective heating of the microchannel test article. To size the thermal load required for the ICH method of diffusion bonding, a simple energy balance was used:

$$\int \left[\dot{m}_A \cdot c_{pA} \cdot \Delta T_{BT} \right] dt = m_{ss} \cdot c_{pss} \cdot \Delta T_{RT} \quad (1)$$

where \dot{m}_A is the mass flow rate of argon, c_{pA} is the specific heat of argon, ΔT_{BT} is the difference between the current temperature and the incoming temperature of the gas, t is time, m_{ss} is the mass of the stainless steel platen assembly and post-heat exchanger tubing, c_{pss} is the specific heat of stainless steel and ΔT_{RT} is the difference between the current temperature and room temperature. This model assumes that all of the heat in the argon flow is transferred directly to the metal mass in the platen assembly and tubing.

Integration of Eq. 1 and rearranging terms yields:

$$T = T_B - \left[e^{\left(\frac{\dot{m}_A \cdot c_{pA} \cdot t}{c_{pss} \cdot m_{ss}} \right)} \cdot (T_B - T_R) \right] \quad (2)$$

where T is the temperature of the metal mass, T_I is the incoming argon temperature and T_R is room temperature. Using estimates for the metal mass and temperature requirements, this model was used to produce the curves in Figure 3.5. For a target ramp time of 15 minutes, an incoming argon temperature of 1000°C and a desired bonding temperature of 900°C, this model suggests a required argon flow rate of 34 SLPM.

To evaluate the thermal distribution within the platen assembly, a simplified two-dimensional thermal model of the platen assembly was used in conjunction with a simple energy exchange calculation to determine the output temperature and flow rate requirements of the heat exchanger (Appendix B). For rough-cut analysis, the fluid was assumed to be incompressible as the pressure drop through the platen assembly was found to be low (around 2 psi). A finite element (COMSOL) model was developed based on Navier-Stokes equations to solve for the gas velocity and an energy balance equation to solve for the steady-state temperature distribution inside the block. Argon was

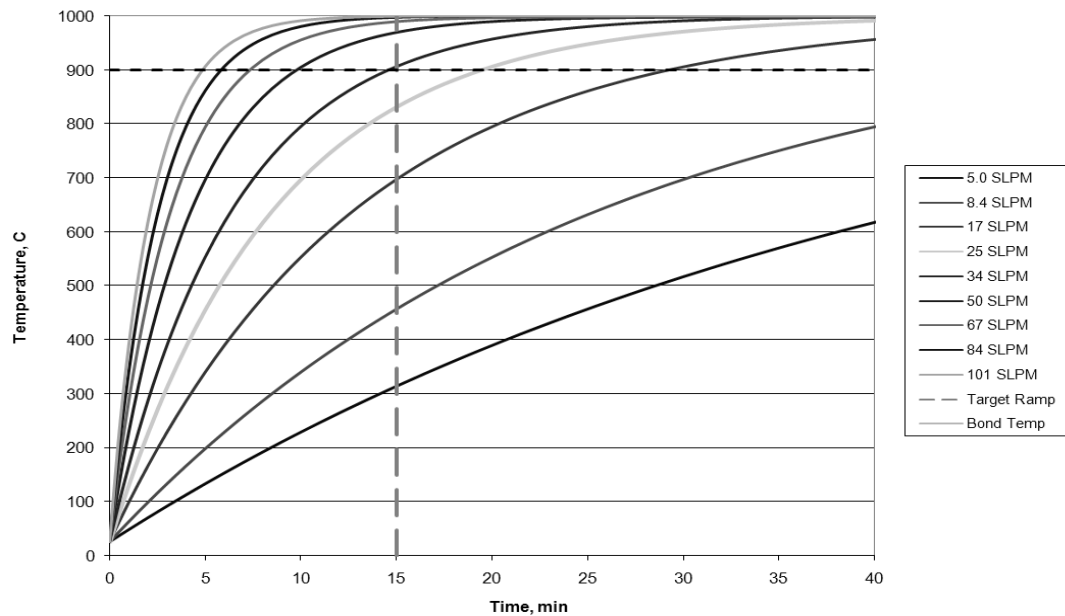


Figure 3.5. The effect of mass flow rate on heating time assuming a fixture mass of 400 grams and an inlet temperature of 950 °C.

specified at a constant velocity at the inlet boundary and at a zero gage pressure at the outlet. A constant temperature boundary condition was used at the outside edges of the insulation (300 °C) and for the fluid entering the assembly. To simplify, a convective flow boundary condition was used along all flow surfaces, constant densities were used for all materials, and a constant viscosity was used for argon. Under these conditions, the analysis found that test article temperatures near the desired bonding temperature (900 °C) could be achieved using an inlet stream of argon at 1100 °C with inlet boundary

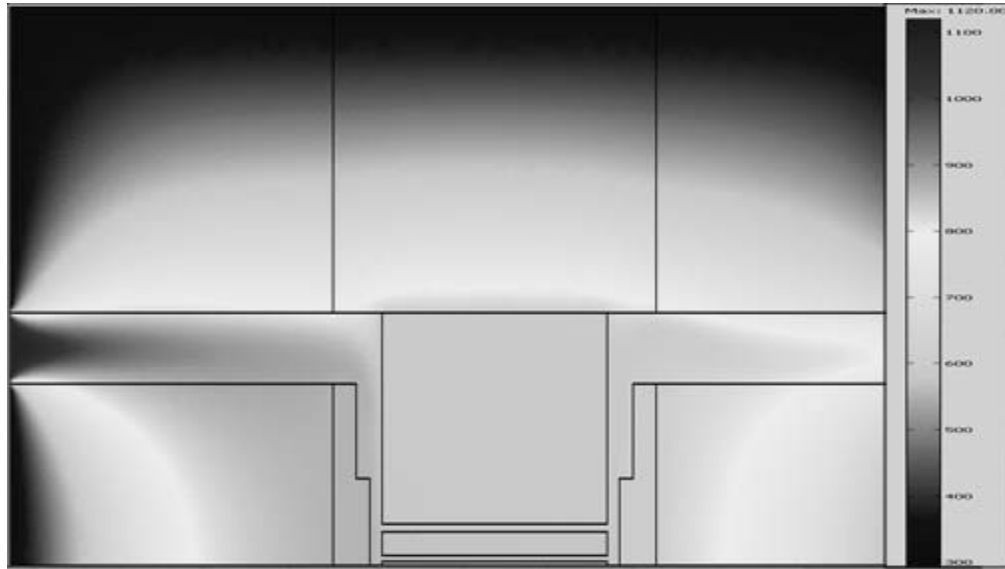


Figure 3.6. Thermal modeling results on ICH using COMSOL

condition of 11.5 m/s. Distribution of temperature across the test article was found to be suitable as shown in Figure 3.6. The design of the heat exchanger is described elsewhere²⁵.

2.2 PLATEN ASSEMBLY DESIGN

2.2.1 Microchannel Test Article

The test article design used in this study is shown in Figure 3.7. It was designed to receive flow from both the top and bottom platens. The test article consisted of seven 316L stainless steel laminae with the following dimensions:

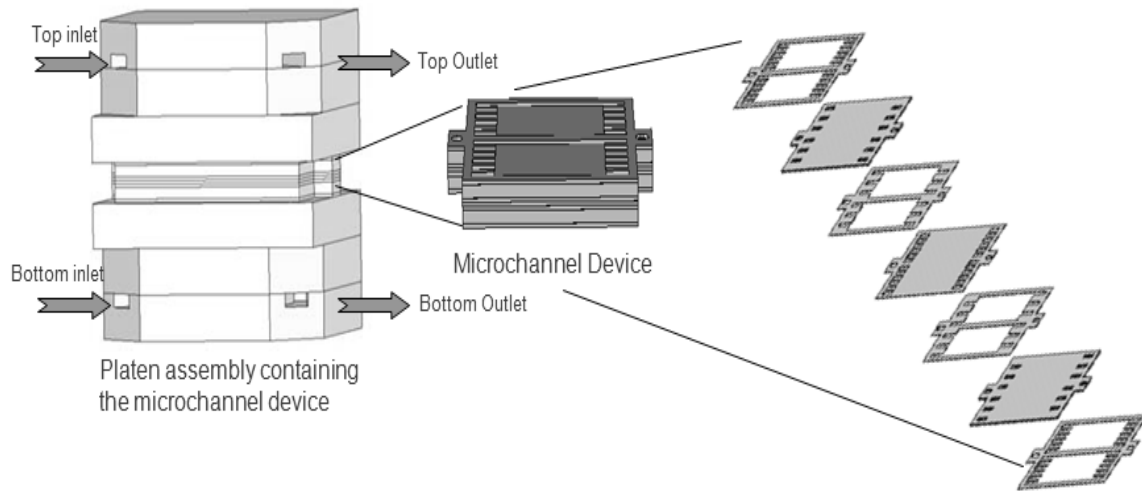


Figure 3.7. Test article architecture

1. End plates (2) dimensions: 25 x 25 x 1.25 mm
2. Channel or flow laminae (4) dimensions: 25 x 25 x 0.375 mm
3. Middle lamina (1) dimensions: 25 x 25 x 0.375 mm

The two outer channel laminae were used to direct the transmission of bonding pressure within the device. In this case, the application of bonding pressure over the channels would lead to significant deflection of the end plates. Patterning of the laminae was carried out with the use of wire EDM from annealed sheetstock.

2.2.2 Platen Assembly

The platen assembly was designed to supply the hot gas to the test article and transmit the bonding pressure from the hydraulic press during the bonding cycle. Figure 3.8 shows an assembly of the test article between the platens. The test article stack is placed and aligned in the platen assembly to receive heat from the argon gas. Platens were made from 321 stainless steel platestock (30.48mm x 30.48mm x 5.08mm) with flow paths machined on the surface of each plate to allow for the passage of argon gas in and out of the test article. Platens were diffusion bonded in a vacuum hot press (VHP) at a pressure of 6900 kPa (1000 psi) and a temperature of 1000°C for 3 hours.

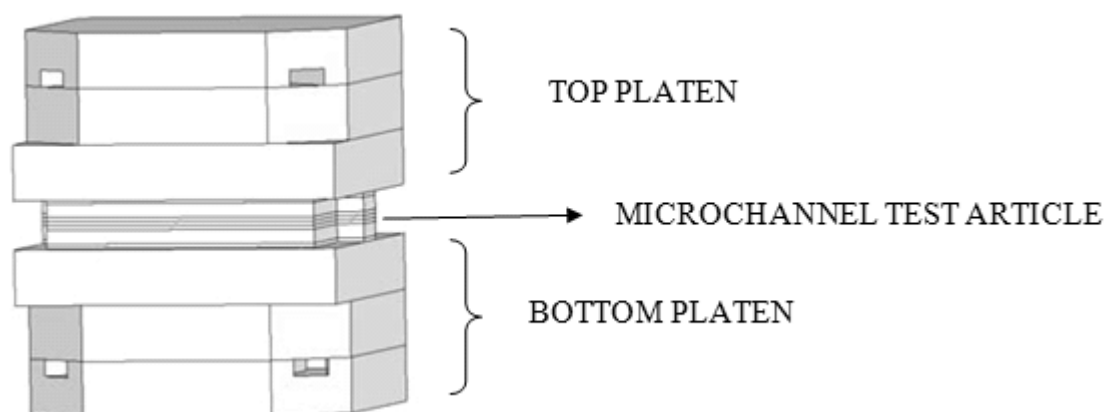


Figure 3.8. Platen assembly design with test article

2.2.3 Leakage Tests

One concern with regard to the safety and economic feasibility of the process was the amount of inert gas which leaked from between the platens and unbonded laminae. The setup for conducting these leakage tests is described elsewhere.²⁵ Here, the results of leakage tests are summarized. Leakage measurements were carried out by varying back pressures on the outlet ranging from 0 to 140kPa (20 psi). The flow rate at the inlet was

maintained at a constant rate of 21.75 SLPM. Volumetric leakage was calculated using the following relation:

$$L = F_{in} - F_{out} \quad (1)$$

where

$L \sim$ Volumetric leakage (SLPM)

$F_{in} \sim$ Flow rate of the gas at the inlet (SLPM)

$F_{out} \sim$ Flow rate of the gas at the outlet (SLPM)

Figure 3.9 shows the variation of volumetric leakage with increasing clamping pressure at different back pressures. The leakage was found to be 1.73% at a clamping pressure of 5520 kPa (800 psi) when there was no back pressure on the outlet line. This result suggests that the clamping pressure needs to be on the same magnitude as the bonding pressure. Prior studies have shown that the application of bonding pressure prior to thermal cycling can generate significant microchannel warpage²⁶. This warpage has

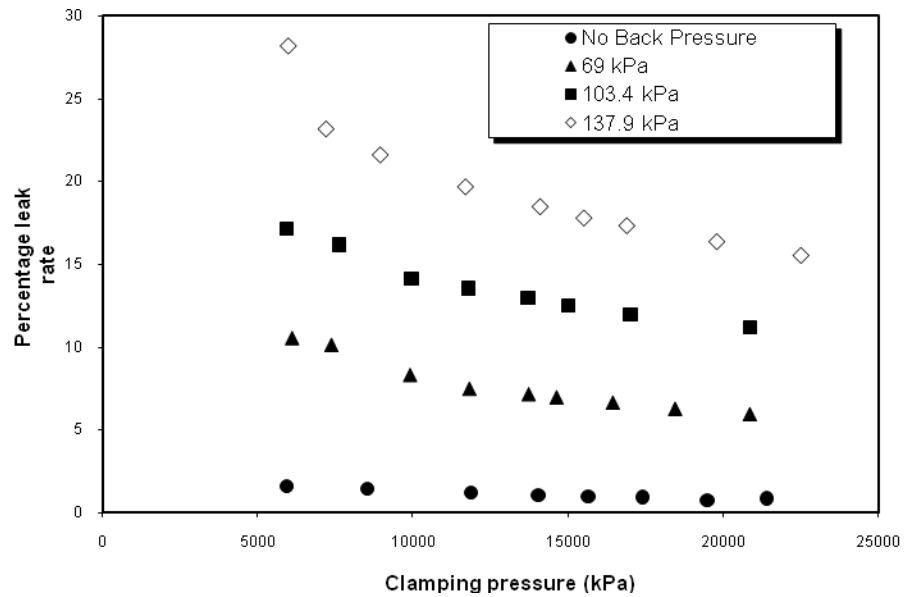


Figure 3.9. Leak rate vs Clamping pressure with varying back pressures.

been found to be due to the differential thermal expansion between bonding fixtures and laminae during ramp up. This finding suggests the need for the bonding platen to be made from a material with matching thermal expansion characteristics. This further confirmed the choice of platen material (321 stainless steel). Volumetric leakage was found to increase with increasing back pressure. Back pressure simulates the type of pressure conditions that might be found in larger devices. It was experimentally determined that 28.2% of the gas leaked when the back pressure was 138kPa psi at a clamping pressure of 5520 kPa. Given that the pressure drop across the current device was nearly 14 kPa (2 psi), this is an approximate simulation of a device with 10X the flow path length. At a clamping pressure of 20.7 MPa (3000 psi) and a backpressure of 138 kPa (20 psi), leakage was found to be approximately 15%. This would be near the upper end of the bonding pressure.

One goal with regard to leakage tests was to analyze the effect of diffusion barriers on leakage. Diffusion barriers are applied to platens to keep the laminae from bonding to the platens. Tests were performed by spray coating a layer of boron nitride particles onto platens prior to running leak tests. As shown in Figure 3.10, the percentage leak rate increased by about 2% with the use of the barrier coating using a back pressure of 69kPa (10psi) which is not significant.

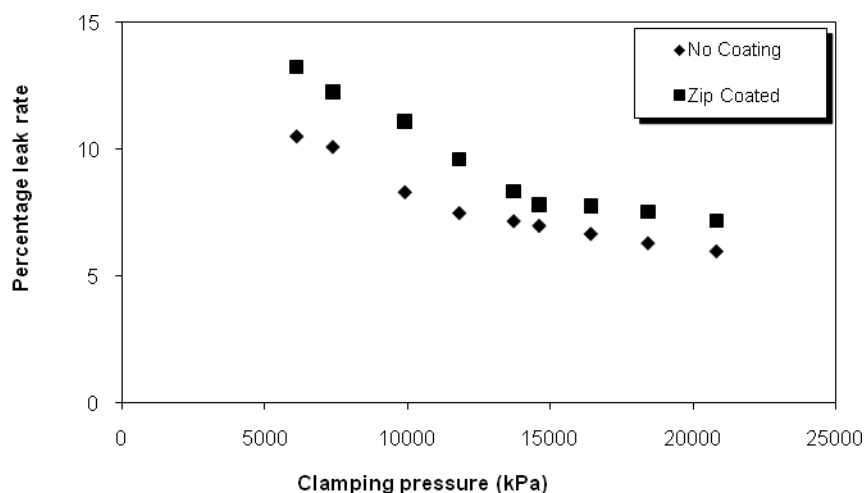


Figure 3.10. Percentage leak rate versus clamping pressure with/without diffusion barrier.

Altogether, these results suggest that for small devices, the rate of Argon loss due to leakage will not become an economical barrier. This is particularly so in light of the fact that production implementation of this method will likely: a) involve recycling of the argon; and b) be done in concert with a furnace to simultaneously heat the exterior of the device. The gas would like be needed for short bursts at the start and finish of the bonding cycle and gas losses would only be incurred at the start. Finally, these low leakage rates suggest that leakage of hot gases will not pose a significant safety issue.

2.2.4 Final ICH Test Setup

Figure 3.11 shows the final internal convective heating (ICH) test setup with all its components. Three electrically resistive “fire-rod” heaters (120V, 1000W and had 0.746 +/- 0.004 diameter, 11” max length) were incorporated into the Inconel heat exchanger for thermal control. The heaters were inserted with tight fits to ensure good

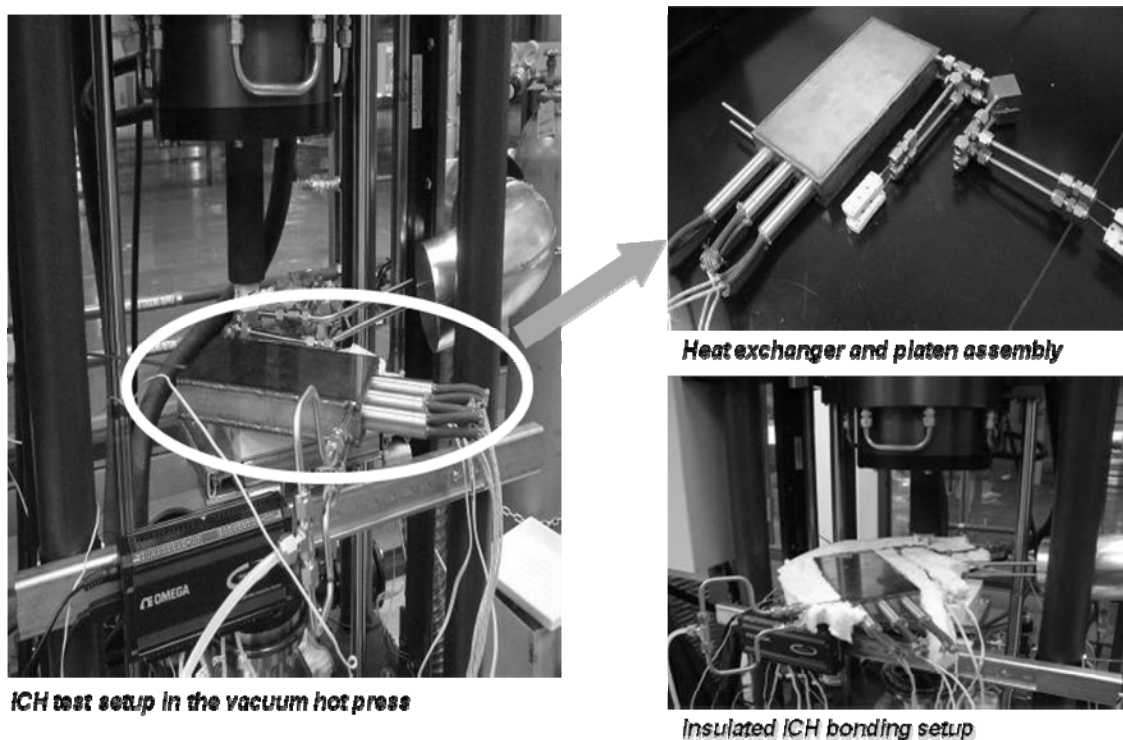


Figure 3.11. Internal convective heating test loop.

heat transfer to the surrounding metal. A Watlow single-loop, auto-tuning temperature PID controller was used to control parameters for optimum system performance. The argon gas flow was controlled using a mass flow controller. Inconel and stainless steel tubing and Swagelok fittings were used to route both hot and cold gas streams. The outlets of the heat exchanger were coupled with the inlets of the platen assembly using T-type 1/4" inconel couplings.

KMQIN-032U-6 type thermocouples with diameter of 0.032" were inserted into the platen assembly. Inlet and outlet thermocouples were snaked to the inlets and outlets of the platen assembly to improve the accuracy of temperature measurement. A K type thermocouple was placed at the outlet of the heat exchanger. The entire assembly was mounted on a strut mount clamp made up of zinc plated stainless steel for withstanding high temperatures. The ducting provided near the hot press received the hot gas, mixed it with air and sent it out into the exhaust.

2.3 EXPERIMENTAL DESIGN

To evaluate the effectiveness of the ICH method, an experiment was conceived to compare diffusion bonding results using ICH and VHP methods under identical processing conditions. Final bonding conditions were: bonding pressure = 24.13 MPa; bonding temperature = 900°C; heating rate = 20 °C/min; cooling rate = 20 °C/min; and time at bonding temperature = 2 hours. Gas flow rates for ICH cycles were maintained at 21.7 SLPM. Vacuum pressure within VHP cycles was held to 10^{-4} torr. Bonded test articles were tested for device leakage, percent voids on the bond line and microchannel warpage. These tests are described in more detail below.

Final bonding conditions were chosen based on the results of preliminary testing showing greatly differing amounts of microchannel warpage produced when using the ICH and VHP methods under these conditions. To ensure that the microchannel warpage detected was not due to creep or other failure mechanisms at the bonding temperatures and pressures, an initial test article was produced at the same bonding temperatures and pressures using greatly reduced heating and cooling rates (8 °C/min). Figure 3.12 shows metallographic cross-sections of a test article bonded under these conditions. The sample shows very little warpage ($1.8 \pm .07 \mu\text{m}$) with few voids on the bondline (0.27%). No “barreling” of features is found suggesting that creep is not present.

2.4 EXPERIMENTAL PROTOCOL

Experimental protocol consisted of three stages: pre-bonding, bonding and post bonding. These stages have been described in this section.

2.4.1 Pre-Bonding Protocol

For both sets of experiments, bonding pressure was controlled with the use of a hydraulic ram within a vacuum hot press. During ICH cycles, the hydraulic ram was operated without the use of vacuum vessel. Prior to all experiments, the hydraulic press was calibrated by verification of output force readings using an analog load cell. Temperature was controlled using VHP controls and the ICH temperature controls described above. Calibration of thermocouples was performed using a furnace. Environmental conditions were controlled by the percent oxygen in the inert gas and vacuum pressure within the VHP.

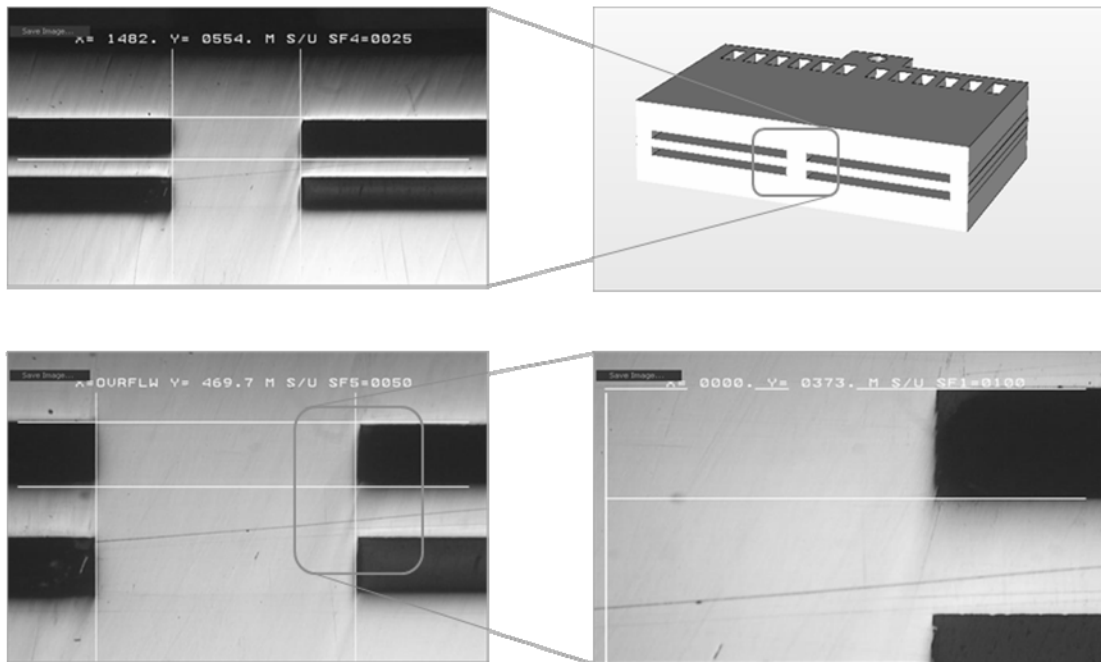


Figure 3.12. VHP sample produced with typically low heating and cooling rates showing low void fraction and well defined microchannel geometries.

All samples were characterized and cleaned prior to bonding. The same lot of annealed, cold-rolled stainless steel 316L was used for both VHP and ICH test articles. Parallelism and surface conditions of all laminae were measured before each bonding cycle using a Veeco profiler. The profiler was calibrated using surface roughness or step height standards. Surface profiling included taking five scans at different places on the test article surface for roughness, three scans at different edges for burr height and one 2 cm scan in the middle of the laminae. Average middleline roughness was found to be $0.32 \pm 0.09 \mu\text{m}$ for ICH samples and $0.34 \pm 0.06 \mu\text{m}$ for VHP samples. Average burr height was found to be $8.2 \pm 2.3 \mu\text{m}$ for ICH samples and $7.73 \pm 3.4 \mu\text{m}$ for VHP samples. Parallelism across a 2 cm scan was found to be $4.8 \pm 0.7 \mu\text{m}$ for ICH samples and $4.67 \pm 0.4 \mu\text{m}$ for VHP samples. The cleaning process involved four steps: the removal of oxides using a citranox agent; grease removal using acetone; removal of residues using ethanol; and application of de-ionized water for final rinse.

2.4.2 In-process protocol

For ICH, the thermal cycle was controlled by the PID controller connected to the thermocouples adjacent to the platens and the resistive heating elements. For VHP, two thermocouples situated within the heating zone were used to validate the temperature cycle. One thermocouple was placed on the graphite tooling adjacent to the platen surfaces. For all cycles, bonding pressure was controlled using the hydraulic ram on the VHP. For ICH cycles, bonding pressure was applied at the start of the cycle to act as clamping pressure necessary to minimize gas leakage. For VHP cycles, bonding pressure was applied after the graphite platens had been heated to the bonding temperature to minimize any effects from differential thermal expansion. For ICH cycles, gas flow rates

remained constant throughout the bonding cycle. For VHP cycles, vacuum pressure was monitored as a function of time during the bonding cycle.

2.4.3 Post-Bonding Protocol

After bonding, leakage of the final test articles was investigated by submerging the test articles under water, pressurizing the test articles with air to 241 kPa (35 psi) and searching for bubbles on the perimeter of the device. After leakage testing, metallography was performed on all test articles to investigate void fraction and microchannel warpage.

Figure 3.13 shows the flow shim of the device that has been used to demonstrate metallographic sections on the device. Three different cross-sections were used to investigate warpage, void

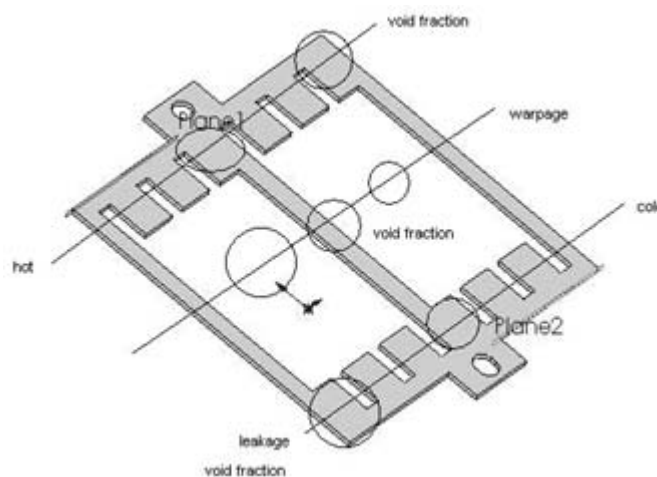


Figure 3.13. Flow shim of microchannel test article

fraction and leakage trends. This is described in detail in the following sections.

Figure 3.14 shows the various sections and their profiles for final sectioned test articles. Measurements for void fraction on the bond line and microchannel warpage were performed consistent with prior papers²⁶. Two void fraction and warpage measurements were taken on the front, back and centre of each section. These measurements were coordinated with the scheme in Figure 3.14 as to whether the measurements were in the inlet, channel or outlet sections of the test article as well as the front, middle and back of the test article. For ICH samples, the front of the test article was considered the side on which the argon gas entered and exited. For VHP samples, the front of the test article was considered the side facing the front of the VHP.

Altogether, six measurements (void fraction and warpage) were taken from each

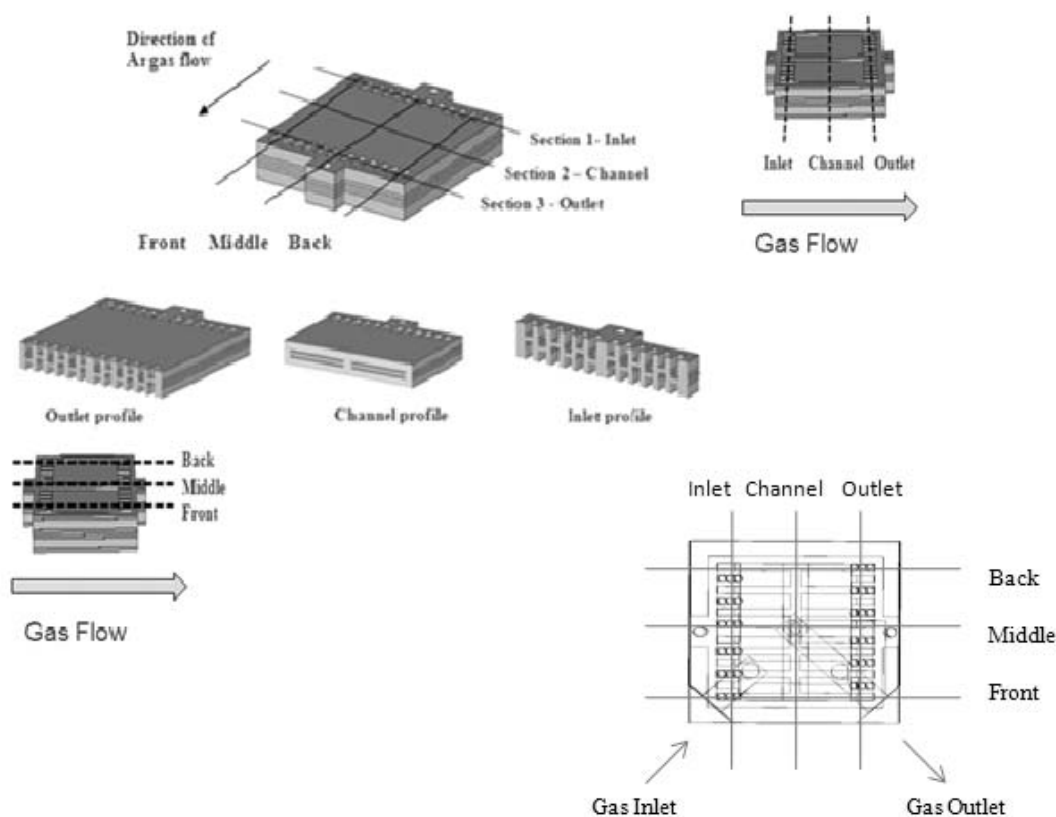


Figure 3.14. Sectional views of microchannel test article

section of each test article for a total of 18 measurements per test article. A total of six samples were sectioned; three ICH-bonded samples and three VHP-bonded samples. Consequently, a total of 108 measurements were taken for both void fraction and warpage measurements. Statistical analyses were performed to assess whether the means of the two sets of samples were statistically different.

3 RESULTS AND DISCUSSION

All test articles were found to be leak tight at 241 kPa (35 psi) of air. (Results of

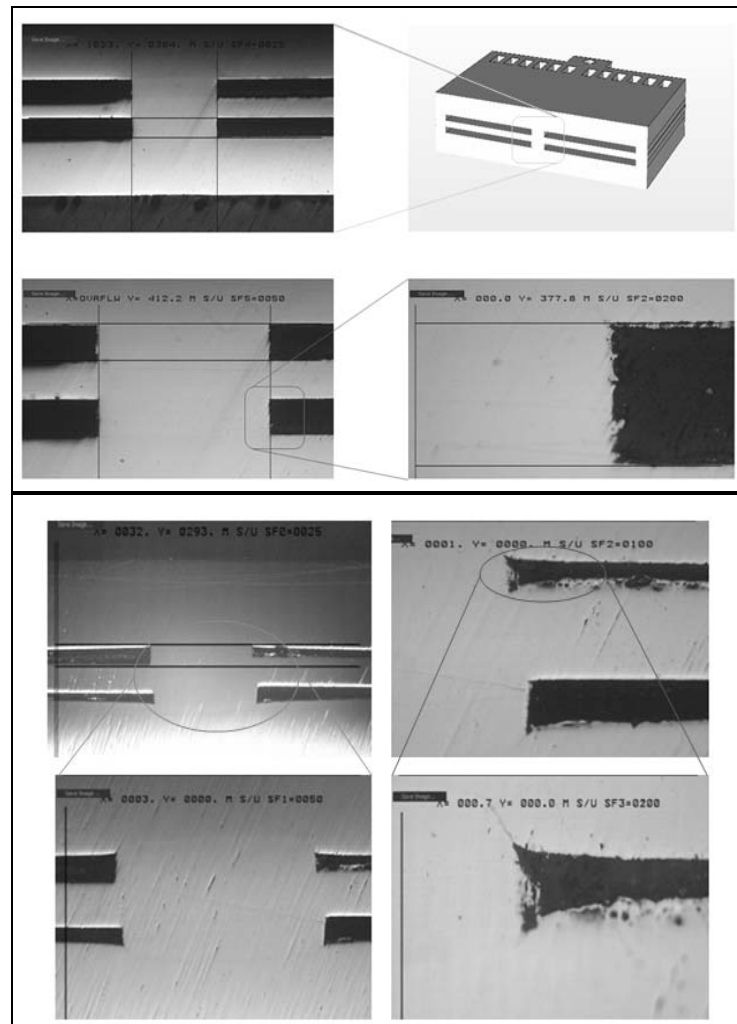


Figure 3.15. Metallography results for test articles produced using (top) ICH and (bottom) VHP methods. Channel height for the test article design is 375 μm .

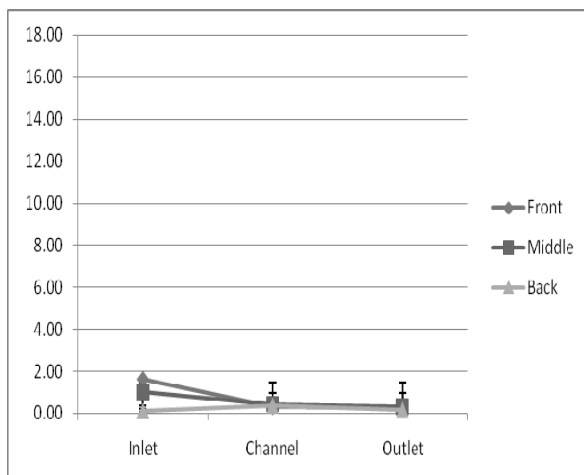


Figure 3.16. Warpage in ICH samples

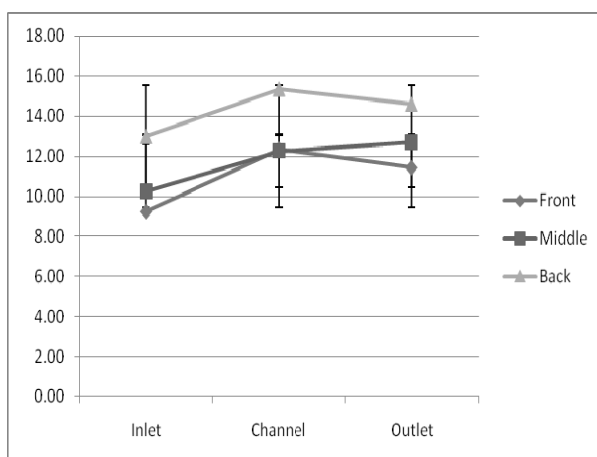


Figure 3.17. Warpage in VHP samples

leakage tests are given in Appendix C.)

Results from metallographic sectioning showed that microchannel warpage within the ICH test articles was much lower than in VHP test articles. Figure 3.15 shows archetypal micrographs within test articles produced using ICH

and VHP protocol, respectively. In general, VHP-processed samples show greatly deformed microchannel geometries when compared with respective ICH samples.

Figures 3.16 and 3.17 provide a quantitative comparison of warpage in the ICH and VHP test

articles. Test article location refers to the front, middle, and back regions of inlet, channel, and outlet cross-sections (defined based on Figure 3.14). For comparison purposes, all warpage measurements were taken on the same 1 mm spans within the same regions of the test articles. Average warpage within ICH samples is $1.4\% \pm 0.7\%$ compared with VHP samples at $12.49\% \pm 1.48\%$. The ICH results are excellent. Prior heat exchanger effectiveness studies have shown that for channels of this dimension, channel variations below 5% have very little effect on heat exchanger effectiveness while variations of 20% can require as much as 50% increase in heat exchanger size²⁷.

It is important to note that the deformation in Figure 3.15 (bottom) is not indicative of creep which is further substantiated by the results in Figure 3.12 which were produced at the same bonding temperature, pressure and time at bonding temperature. ICH samples compare favorably with test samples in Figure 3.12 produced by VHP (warpage of $2.66\% \pm 1.8\%$). The differences between Figures 3.12 and 3.15 (bottom) are the rates of heating and cooling. Therefore, it is expected that these deformations are due to larger thermal gradients caused by the VHP protocol. This is explained below.

Inside the VHP during heating, heat is transferred from resistive heating elements to the surface of the test article by radiation and then to the middle of the test article by conduction. Heat is conducted over a distance greater than 25 mm. By contrast, in the ICH protocol, heat is transferred from the argon gas to all internal surfaces and then to the middle of the adjacent mass. In the case of a microchannel surface, the distance to the middle of a microchannel fin is roughly 0.187 mm. Therefore, the conduction distance in the ICH protocol is less than 1/100th the conduction distance in the VHP protocol. When the heating (or cooling) rate is increased, the conductive heat transfer becomes a bottleneck in the heat transfer process causing a buildup of energy and, consequently, an ever larger thermal gradient. In the VHP, this buildup happens at much slower heating rates than in the ICH method.

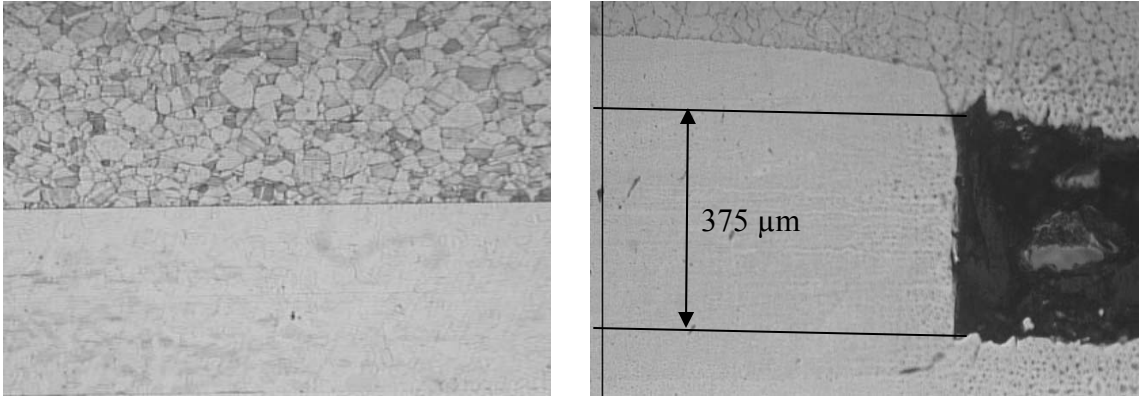


Figure 3.18. Cross sections of ICH(left) and VHP (right) using aqua regia etch

Figure 3.18 shows cross-sections of ICH and VHP samples prepared with an aqua regia etch. The cross-section shows large equiaxed grains typical of a long heat treatment with bondlines having no void fraction. Average percentage void fraction within ICH samples was $2.32\% \pm 0.69\%$ compared with VHP samples at $0.18\% \pm 0.26\%$ indicating a small increase in the number of voids within ICH samples. This difference is likely due to the effects of inert gas leakage across the bondline during ICH processing.

Further, some interesting trends were found in the void fraction data for the ICH samples. Figure 3.19 is a 3D representation of the void fraction data from sections taken from similar regions of the ICH and VHP test articles. Noticeable in Figure 3.19 (left) is

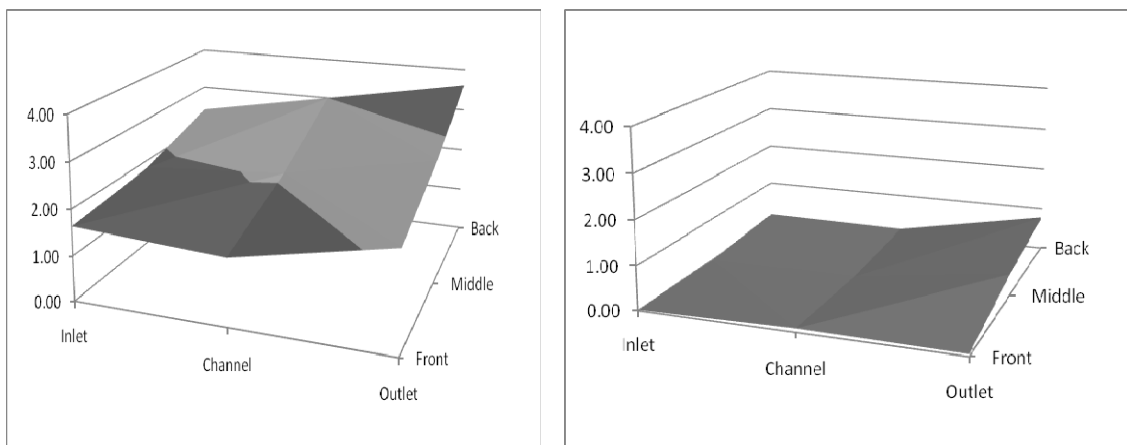


Figure 3.19. 3D representation of average % void fractions in ICH (left) and VHP (right) in different regions.

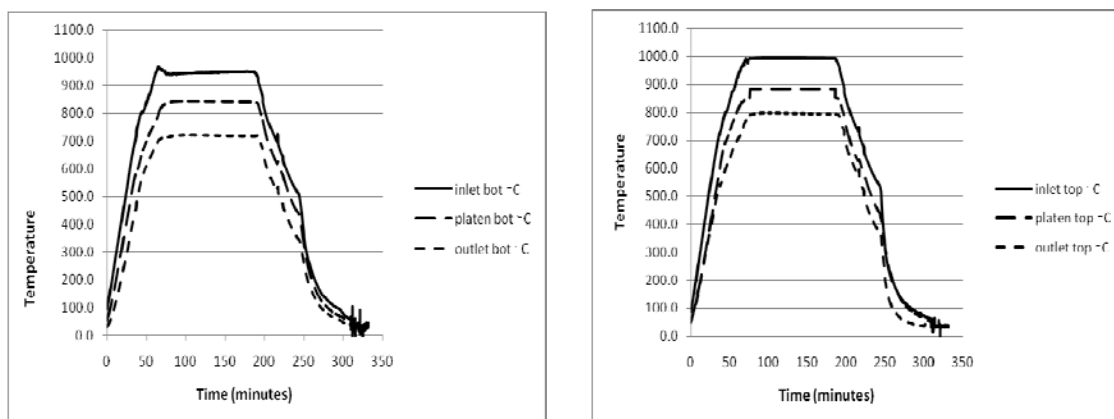


Figure 3.20. Data generated by thermocouples in the ICH test loop

an increasing trend of void fraction from the front inlet to the back outlet of the device. This trend was not found in the VHP samples, which showed minimal voids at any region of the test article. It is expected that the ICH trend is due to higher bonding temperatures at the front inlet. As shown in Figure 3.20, the inlet was at a higher temperature during ICH processing. Further, as shown in Figure 3.14, the front of the platen assembly is the side from which the argon stream entered and exited. Therefore, it would be logical that the front of the platen assembly as a whole was warmer than the back of the platen assembly. Figure 3.21 shows a 2D plot of ICH void fraction data with error bars suggesting additional data would be needed to verify this claim. Evidence of thermal gradients within the platen assembly suggests the need for better thermal insulation.

Void fraction trends in the ICH test samples could also be explained as a result of generally

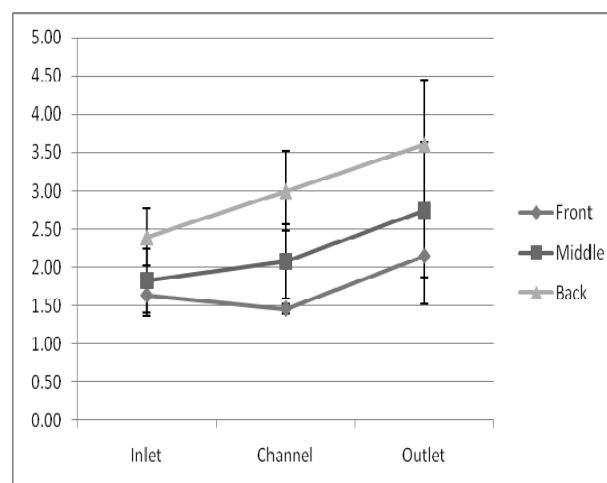


Figure 3.21. 2D plot showing average void fractions in ICH samples

poorer parallelism within the ICH platen assembly stack than in the VHP. The ceramic insulating blocks that were positioned above and below the ICH platen assembly were difficult to machine. Any out-of-parallelism could have led to poor stress distribution within the test article. However, this is a less likely explanation than the temperature gradient explanation above since pressure sensitive films were used to check the parallelism between platens and the test articles prior to bonding.

Figure 3.22 shows the thermal profile generated by the thermocouple placed in

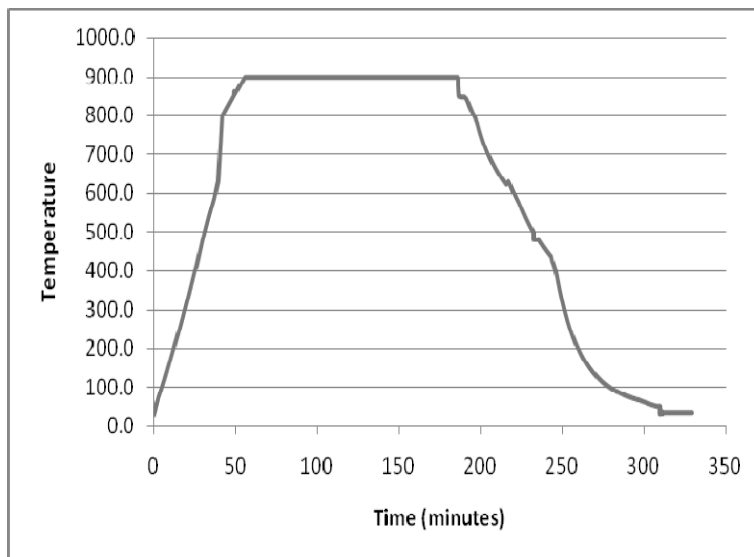


Figure 3.22. Thermocouple data from VHP final conditions

the graphite block during the VHP bonding cycle. A comparison of Figures 3.20 and 3.22 shows that the average bonding temperature of the ICH test articles (represented by platen top and platen bottom) were lower than

those of the VHP test articles. This would explain the generally higher void fraction on the bondline of the ICH test articles. Ramp up rates were nearly equal roughly $17^{\circ}\text{C}/\text{min}$ and the ramp down rate was nominally $15^{\circ}\text{C}/\text{min}$. Noticeable in both graphs is an increase in cooling rate below 500°C . In the case of the ICH process, this was the temperature at which the insulation was removed. For the VHP case, helium was introduced at this temperature.

4 CONCLUSIONS

This paper has demonstrated a new internal convective heating (ICH) technique for the diffusion bonding of metal microchannel arrays. The ICH technique is capable of bonding microchannel laminae with little warpage and low bondline void fractions under shorter bonding cycle time conditions compared with conventional vacuum hot press methods. Results suggest that this may be due to smaller thermal gradients within microchannel devices during the ICH bonding cycle. Limitations of this process include device size both due to leakage of inert gas at higher pressure and thermal loss of the gas. It is expected that leakage can be managed for larger devices using manifold inlets and outlets. It is also expected that thermal loss can be managed with better insulation.

4 SUMMARY

The objective of our research was the development of an internal convective heating (ICH) method for reducing the bonding cycle time within the diffusion bonding of arrayed microfluidic devices. Preliminary research investigated the leakage and thermal requirements for diffusion bonding microchannel arrays via ICH and substantiated that the costs associated with the ICH of small devices are manageable. It is suggested that this can further be improved through the recycling of the inert gas and recuperation of the waste heat.

Further, the method of ICH was successfully demonstrated to reduce the cycle time in diffusion bonding techniques compared to traditional VHP methods. The data generated from six bonded samples proved that the ICH protocol will allow faster heating and cooling than VHP protocol. Larger thermal gradients were suggested as the cause for microchannel warpage in the VHP based on available data.

Several suggestions are made for improvement of the ICH method. It is expected that the ICH method would perform better within a furnace enclosure. This would not only provide better isolation from the ambient but provide better thermal insulation and better safety for the users. Also, it is expected that there may be higher levels of oxide inclusions to go along with higher void fractions within ICH samples. Forming gas could be used to replace the inert gas to perhaps reduce voids and oxides.

APPENDIX A

LITERATURE REVIEW

Microlamination is a commonly used technique for the manufacturing of bulk microfluidic devices. It involves patterning, registration and diffusion bonding. Various techniques have been used for the patterning of fluid layers. Good feature resolutions can be achieved with photochemical etching. The laminae can be etched either single-sided or double-sided to achieve complex cavity shapes. Direct-writing methods like laser machining offer higher flexibility in the production of substrates compared to photochemical etching. Stamping of patterns are an alternative to laser machining for mass production, if channel features are not too small. High precision is required in the z-axis for metals. This is controlled by cold rolling process, which is traditionally known for precise, high-volume production (e.g. process is used to make shim stock). In a typical microchannel array, the lateral patterns on laminae are much larger requiring less precision. For the patterning of very complex channel features in metallic substrates, fabrication methods like electrochemical micromachining (ECMM) or electro discharge micromachining (EDMM) could be of potential interest. Wire-EDM is capable of cutting hundreds of layers at the same time by stacking up the substrates. After patterning and cleaning of the individual fluidic layers the bonding process follows.

Diffusion bonding is commonly used to join metallic and ceramic structures. A critical step during the bonding of the patterned layers is the proper alignment and registration of the layers relative to each other. Commonly, alignment of the layers is achieved with pins and precise pinholes in the layers. Thomas and Paul have shown an

innovative alignment technique by using the difference in thermal expansion between fixture and laminae. During diffusion bonding laminae are heated up to bonding temperature under an applied bonding pressure and held at these conditions for a period of time necessary to join the layers to a monolithic device due to solid state diffusion. Insufficient bonding conditions can lead to poor bonding and leakage while too great of bonding conditions can lead to deformed or collapsed channel features.

MATERIALS

The application portfolio of bulk microfluidic devices requires that the materials used have thermal, chemical and physical properties of more traditional engineering materials such as metals or ceramics with high melting temperatures and corrosion resistance. Therefore, most commonly used materials are stainless steel, copper, aluminum alloys, titanium, and many others. For high-temperature applications in microreactors, ceramics have been successfully implemented. Other high temperature materials like aluminide foils have been investigated by Paul and Alman et al. for the application in microlaminated high-temperature heat exchangers.

DIFFUSION BONDING

Many researchers have used diffusion bonding to convert stacks of microchannel laminae into bulk microfluidic devices. Diffusion bonding of materials in the solid state is a process for making a monolithic joint through the formation of bonds at atomic level, as a result of closure of the mating surfaces.

The principal parameters activating diffusion bonding are bonding temperature, bonding pressure and processing time. Between temperature and pressure a hyperbolic

relation is recommended to yield sound bonds. Bonding at higher temperatures needs less pressure than bonding at lower temperatures. The bonding process takes place at temperatures below the melting temperature T_m of the lowest melting material, typically at $0.5-0.7 T_m$. The pressure application is such, that macro-deformation of the joined parts is not reached, although increasing the pressure could improve the bonding strength. Typical pressure ranges are 5-10 MPa for carbon steels, 7-12 MPa for stainless steels and 3-7 MPa for aluminum alloys. An optimal bonding pressure is approximately equal to the yield strength of the workpieces at the bonding temperature. Where dissimilar materials are to be joined, the choice of bonding pressure is decided by the weaker of the two materials.

Another critical factor which defines the success of any diffusion bonding cycle is the processing time. The processing time is related to the temperature and pressure parameters used in the bonding cycle. Also, between temperature and pressure a hyperbolic relation is recommended to yield sound bonds. Bonding at higher temperature means the furnace requires more time to heat up, but requires lesser bonding pressure for a lesser time period. On the other hand, bonding at a lower temperature reduces the time on the ramp up, but may mean exposure to pressure for a longer period of time, which in turn results in channel deformation. The bonding time can vary depending on the applied temperature and pressure from several minutes to several hours. An indirect indication that a diffusion process is complete is the ultimate strength of the bond which should be ideally the same as the parent material. The strength of the bond is proportional to the square root of the bonding time, which is characteristic for any diffusion-controlled process. The quality of diffusion bonded joints can be evaluated by using a wide range of

techniques. These include metallography, ultrasonic inspection and the use of mechanical testing procedures such as tensile, impact and lap shear tests. Mechanical testing procedures like tensile testing have been reported as reliable methods for the assessment of bonding quality. However, these methods are not readily applicable to sheet material structures and metallographic techniques can be used by analyzing the fraction of interfacial voids.

Increased surface roughness increases the volume fraction of voids at the bonding interface decreasing the bonding strength. It is also understood that an increased temperature reduces the yield stress of the materials and activates the diffusion and mobility of atoms in the lattice. When both pressure and temperature are applied together, the bonding process can be accelerated.

Vacuum hot presses (VHP) are typically used to implement diffusion bonding protocols for microchannel devices and provide reasonable protection from oxide films and voids in bonded portions. It is used in cases of subjecting materials to high pressing forces over large work areas under high vacuum or inert gas environment at elevated temperatures. Pressure uniformity can be challenging. Further, the VHP often has been undesirably large, having bulky construction with its utilizable enclosed work area disproportionately small to the size of the enclosure or the associated press apparatus. Consequently, the capital expense has sometimes been so large as to impede growth in technology of microchannel devices. Further, the hydraulic vacuum hot press is not always an appropriate machine tool for production of diffusion bonded devices. Finally, the vacuum hot press requires batch operation which restricts the throughput.

ALTERNATE TECHNIQUES

In the past, numerous microchannel based reactors, heat exchangers, and separators within the context of basic and applied research projects have been developed and fabricated, where unit cost is unimportant relative to other factors such as performance, weight, and size. As the need for lighter and/or stronger materials has advanced, interest has heightened in the technology of metal pressing, compacting and joining materials for the fabrication of parts and in metal treating such as, for example, diffusion bonding, powder metallurgy, vacuum brazing and thermo-mechanical processing of materials. The efficiency of these techniques is defined by the factors of cycle time, cost of operation and size. Some of the prior bonding techniques and their efficiency are discussed in this section.

Some of the other alternatives to diffusion bonding include brazing, welding and shrink fitting. While brazing can provide a metallurgical bond, the diffusion of undesirable components such as flux materials from the brazing composition into the adjoining bodies may weaken the surrounding alloys or cause grain boundary attack. These are extremely undesirable for microchannel devices used for heat and mass transfer applications. Brazing and welding can reduce strength by causing re-crystallization of cold-worked metals, averaging of precipitation hardened alloys, and reversing the transformation hardening in some alloys. In steels, martensitic structure may transform back to softer austenite. Thus, the method of pressure welding is advantageous when the process is desired to be automated. However, this method is inept when the eccentricity between the bodies to be bonded is large. Also, welding is not effective when the bodies have complex configurations, which is usually the case with microchannel structures.

Also, the shrink fitting process relies on a tight physical contact to frictionally hold the bodies and is not as strong as either brazing or diffusion bonding as it does not provide a strong metallurgical bond. Bond strengths need to be extremely high as these devices undergo high pressures due to the fluids flowing through them.

A prior diffusion bonding technique avoided the usage of an external ram for the application of pressure during the bonding cycle. As mentioned earlier, Thomas and Paul designed an approach for precise alignment of multiple layers by differential thermal expansion for use in the microlamination process. This process relied upon a positive difference between thermal expansion coefficients of the sub-assembly material compared to the clamping device material to generate the pressure required for bonding at elevated temperatures.

Ultrasonic bonding techniques have also been used in the past, but to a less degree of success due to economic reasons. The super plastic forming (SPF) and diffusion bonding (DB) process is well documented and has been in use in the industry for many years. Conventional compression diffusion bonding uses the force between the opposite die surfaces of the forming press at elevated temperature to achieve intimate contact and pressure between two or more mating surfaces of metal.

OBJECTIVE

This project is aimed at creating new capabilities for the low-cost rapid production of microchannel reactors by addressing one of the longest and most costly steps of traditional lamination processes – the bonding step. Heating and cooling rates in furnace bonding processes are usually limited by the need to minimize thermal gradients within the assembly (shim stack) being bonded. Rapid heating of the assembly by

external heating and intra-assembly conduction leads to significant thermal gradients within the assembly, which can cause shim deformation, channel obstruction, and residual mechanical stresses within the finished part. These mechanical considerations limit the heating/cooling rate to about 5 °C per minute depending upon the size of the hot press and the size of the device being bonded. For bonding cycles that require temperatures around 1000 °C, this represents a very long duration during ramp-up. This problem is further compounded as the size of the bonded device increases. Since the lead time is directly proportional to the cost of the cycle, we decided to target minimizing of the cycle time to significantly reduce the costs of producing such microchannel devices. None of the prior art examined addresses the issue of joining of metals using diffusion bonding at a faster rate, by keeping the ramp-up and ramp-down rates to an extremely low level.

We propose that the internal convective heating (ICH) bonding technique can provide the assembly with rapid heat input while minimizing thermal gradients within the assembly, along with increasing the ramp up/ramp down rates. As compared to traditional diffusion bonding methods, it is conceivable that internal convective heat could bring the system up to the bonding temperature in a lot less time depending upon device and process constraints such as thermal gradients allowable within the stack. Heating and cooling times on this order should lead to a significant cycle time reduction as compared to the vacuum hot press.

The ramp up/down rates on the ICH are significantly higher than those on the VHP. The device will be convectively heated to around 1000⁰ C, which is the standard bonding temperature for stainless steel; the material used for our microchannel device.

The constant temperature region is where the bonding pressure is applied and diffusion bonding of the device takes place. One of the challenges of the ICH approach is the potential for gas leakage during bonding. Too high of a leakage rate could factor into the economics as well as the safety of the process. To deliver the necessary heat at proper flow rates, we designed and manufactured a thermal system (a microchannel heat exchanger) which heats the convective fluid and controls the heating and cooling rates of the entire system.

APPENDIX B

TEST SETUP

Figure B1 shows the conceptual description of the ICH test loop with cross marks representing the spots where thermocouples were placed. Ultra high purity argon was supplied to the system using a gas tank. The required flow rates were provided using a calibrated mass flow controller which has a closed loop control system which was given an input signal that it compares to the value from the mass flow sensor and adjusts the proportional valve accordingly to achieve the required flow. The flow rate is specified as a percentage of its calibrated full scale flow and is supplied to the MFC as a voltage signal. A pressure sensor was also used to provide an estimate of the back pressures in the system. The argon gas was then supplied to the inconel heat exchanger described

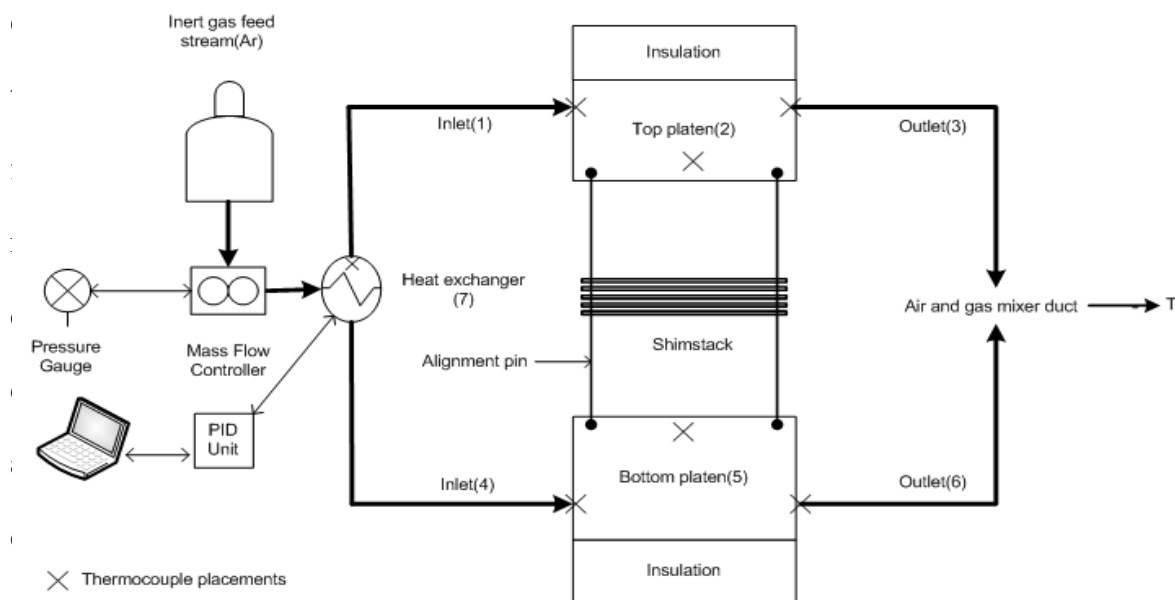


Figure B1. Conceptual ICH diagram with thermocouple placements and PID loop

The figure shows the areas where thermocouples were placed in the platen assembly. Omega's quick disconnect thermocouples with Miniature Connectors are high

quality, economical thermocouple probes. They feature a glass filled nylon connector which is rated for temperatures up to 220°C (425°F). The probes are available in with diameters as small as 0.25mm (0.010 inches) and as large as 3mm (0.125 inches). KMQIN-032U-6 type thermocouple with diameter of 0.032” was used in our experiments.

Type K (chromel–alumel) is the most commonly used general purpose thermocouple. It is inexpensive and, owing to its popularity, available in a wide variety of probes. They are available in the $-200\text{ }^{\circ}\text{C}$ to $+1350\text{ }^{\circ}\text{C}$ range. 6 such thermocouples were labeled and placed at different spots in the platen assembly to get an estimate of the actual temperatures in the device. In the flow loop, 4 of these were placed at the inlet and outlet tubing on both the top and bottom platen. 1/16” holes were drilled in the platen assembly near the test article on the platens and two thermocouples were placed on these to get a reasonable estimate of the temperature on the device. These two thermocouples were not in the flow loop; instead they were monitoring the temperature in the metal. The feedback from these thermocouples was received by data acquisition software which directly provides the data to the computer for analysis. The thermocouple data is going to be critical because the any temperature differences at different zones will account for the bond quality in that particular region in the test article. Before running the final ICH cycle, it was critical to estimate the leakage rates in the flow loop. A high gas leakage rate would result in heat losses as well as create a safety hazard. The leakage tests would also provide us with the minimum clamping pressure required to prevent leakage from the platen assembly.

For proof-of-principle testing, it was decided that the bonding pressure could be supplied by the hydraulic subsystem of a vacuum hot press. This requires the internal convective heating test stand to be set up adjacent to a VHP and operated within the work envelope of the system. In the current test stand, the work envelope is constrained to a maximum of a 75 mm diameter. During warm-up, the purpose of the clamping mechanism is to provide enough pressure to keep the heat exchange gas from leaking out between the shims. During the bonding cycle, the pressure is required for solid state diffusion across faying surfaces. Typical pressures of 1000-1200 psi are required during the bonding step. Heat losses through the system were a cause for concern in the ICH test loop. We decided to use a ceramic insulation which would not only prevent heat loss but also transmit the pressure from the hydraulic rams to the platens assembly.

Material description

Type ZIRCAL-95 Refractory Board is produced from a combination of natural organic fibers and inert reinforcing fillers in a high density calcium silicate hydrate matrix. Designed as a substitute for asbestos cement boards, ZIRCAL-95 is useful as structural and electrical insulation in applications with temperatures to 1100°C (2000°F). ZIRCAL-95's surface is sanded smooth. It has a uniform consistency making it a useful source for custom machined insulating parts.

Fabrication

Zircal 95, 24"x 48" x 1" SS23-A. Zircal-95 has unique machining characteristics. It is easily cut with hand held woodworking tools using slow cutting action. Operator will notice the rate of material removal decreases as increased force and tool speed is applied.

When sawing by hand, a slow steady motion works best. Due to the high parallelism requirements, Zircal-95 was successfully machined using equipment with a diamond sawing wheel, approximately 250 mm diameter with 12 mm long teeth spaced 25 mm apart at 1800 RPM. The ceramic was used for supporting the heat exchanger as well as insulation of the platen assembly.

1. Two Ceramic Block of dimensions 10”x 5” x 1”

The inlet heat exchanger was placed on these blocks, which in turn was placed on a tray or a shelf. The block will absorb the heat that will be produced by the heat exchanger. The heat exchanger was also isolated with a separate insulating material.

2. Two Ceramic blocks of dimension 1.25”x1.25”x1”:

These blocks were placed on either side of the platen assembly and will be in direct contact with the rams of the vacuum hot press. A high amount of precision was

Table B1. Material properties used for COMSOL model

Property	Insulation	SS316	Argon
Thermal conductivity [w/(m*K)]	0.26	$0.0150 \cdot T + 9.250$	0.1415
Density [kg/m ³]	128	8027	0.2370
Heat capacity [J/(kg*K)]	1000	500	828.9

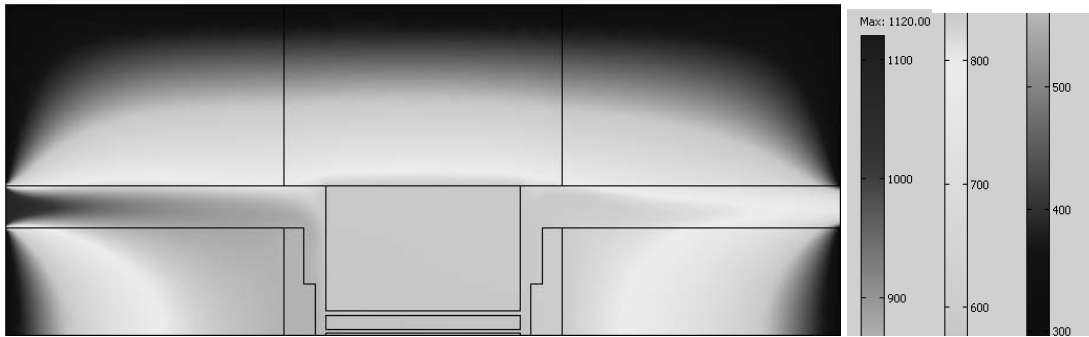


Figure B2 .Thermal modeling results on ICH

required for machining these ceramic blocks as the parallelism of the blocks could majorly affect the diffusion bonding process. Pressure transmission was dependent on the flatness and parallelism of these blocks because even a slightly non-parallel block can result in non-bonded regions in the device.

A two-dimensional thermal model of the platen assembly in cross-section was developed to size the heat exchanger (Figure B2). The middle block (yellow) simulates the top platen made of stainless steel and the top block simulates the insulating block. Thermal and physical properties of the materials are shown in Table B1. The Reynolds number within the inlet and outlet is 600 suggesting laminar flow within the device. Consequently, the model was implemented in a finite element package (COMSOL) using Navier-Stokes equations to solve gas (argon) velocity and an energy balance equation to solve the steady-state temperature distribution inside the block. For the above model, argon was specified at a constant velocity at the inlet boundary (11.5 m/s) and at a zero gage pressure at the outlet. A constant temperature boundary condition was used at the outside edges of the insulation (300 °K) and for the fluid entering the assembly (1120 °K). A convective flow boundary condition was used along flow surfaces. Fluid incompressibility was assumed as the pressure drop through the stack was found to be relatively low. For sizing purposes, a constant density and viscosity of the argon gas was

also assumed. Under these conditions, the temperature within the stack was found to be approximately 850 °C which is close to the final bonding temperature of the device.

Thermal stresses during diffusion bonding

The purpose of this study was to generate the temperature fields in the bonding assembly using finite element method. Not many research papers have been published in connection with temperature distribution and thermal stresses in stainless steel microchannel

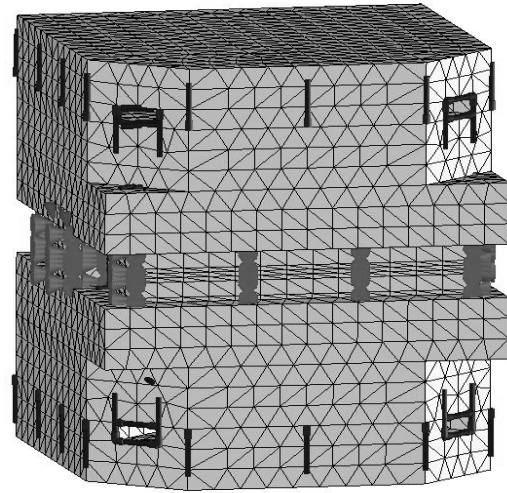


Figure B3. Finite Element mesh of the platen assembly

devices. To validate our design concept, a simple modeling and experimental investigation into the use of internal convective for bonding of laminated structures without use of furnace or hot press was performed. The purpose of the thermal model was to ensure that the microchannel device would be heated to the bonding temperature so that the pressure can be applied to the stack to ensure a diffusion bonding cycle. The thermal profile on the microchannel device would provide an estimate of the stresses caused due to the variable heat in the component.

Overview of model

The internal convective heating bonding cycle is based on the phenomena that hot argon gas enters the platen assembly inlet at the bonding temperature and convectively heats the laminae stack to 1000 C and leaves the system. However, during the first

experimental run on the ICH bonding cycle, a thermal gradient of 200 C was measured from the inlet to the outlet of the platen assembly. The possible reason for the gradient could have been the lack of proper insulation. We have based our thermal model on this observation that a significant thermal gradient exists from the inlet to the outlet of the stack. Our primary goal was to determine the effect of this thermal gradient on the microchannel device. Finite Element Analysis (FEA) provides a reliable numerical technique for analyzing engineering designs. The process starts with the creation of a geometric model. Then, the program subdivides the model into small pieces of simple shapes (elements) connected at common points (nodes). Finite element analysis programs look at the model as a network of discrete interconnected elements. Figure B3 shows the meshed component with the boundary conditions that were used before the generation of the thermal model. The green arrows show the convective heat transfer component of the model where as the blue arrows show the regions where a temperature profile was applied to the solid model.

No. of nodes: 29959

No. of elements: 17050

Coefficient of heat transfer

and boundary conditions

Before modeling the stack, it was critical to calculate the heat transfer coefficient of Argon in the stainless steel platen assembly channel. There

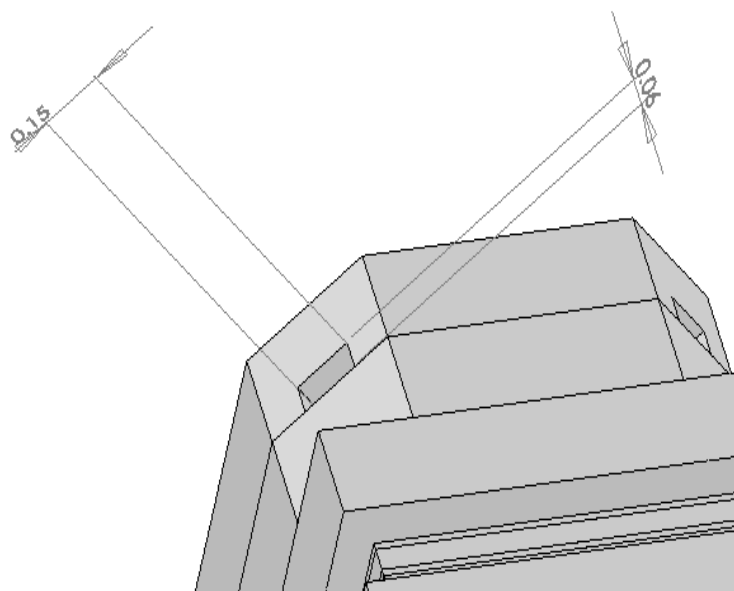


Figure B4. Platen assembly channel dimensions

are numerous correlations for calculation of heat transfer coefficient in different heat transfer modes, fluids, flow regimes, and under different thermo-hydraulic conditions. Often, it can be estimated by dividing the thermal conductivity of the convection fluid by a length scale. In our case, the heat transfer coefficient was calculated from the Nusselt number (a dimensionless number).

Coefficient of heat transfer:

$$h = NuT \cdot k / Dh$$

Platen assembly channel dimensions

Width= 0.15 inches

Height: 0.06 inches

$Dh = 0.00216$

$k = 0.0351 \text{ W/m.K (Argon); } NuT = 0.5322[5]$

$$h = 8.64 \text{ W/m}^2\text{K}$$

Convection describes the heat transfer mechanism between a solid face and an adjacent moving fluid (or gas). It involves the combined effects of conduction and the moving fluid. Fluid particles act as carriers of thermal energy. A solid loses thermal energy through a face with convection if the temperature of the face is higher than the bulk temperature. The solid gains thermal energy if the temperature of the face is lower than the bulk temperature. The temperature of an entity with a prescribed temperature remains constant at all times. Depending on other thermal loads and restraints, the model can lose or gain thermal energy at locations with prescribed temperatures.

The boundary conditions used for the development of the thermal model using COSMOS flow works are as follows:

$$T_{\text{inlet}} : 1000\text{C}$$

$$T_{\text{outlet}} : 800\text{C}$$

Heat transfer mechanism in the device was set to the convective mode and the heat transfer coefficient was: $h = 8.64 \text{ W/m}^2\text{K}$

Thermal modeling results

The inlet and outlet flow paths were set to the temperatures of 1000C and 800C

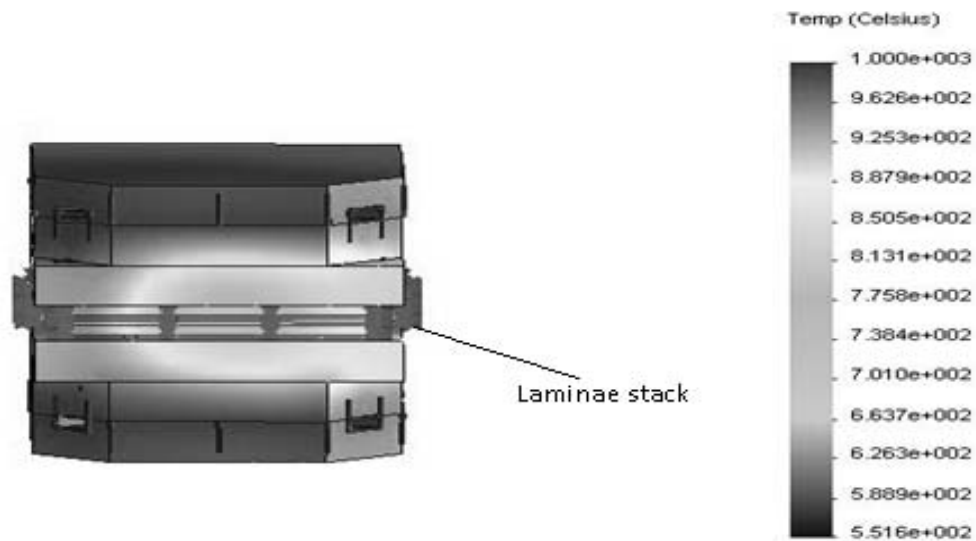


Figure B5. Thermal model of platen assembly

respectively. The ICH concept states that the microchannel device within the assembly gets heated convectively and was therefore simulated using the convective heat transfer

module. The solid model of the platen assembly was used to generate the thermal profile of the stack. The results of the thermal model generated are shown in figure B4. A temperature drop at the central region of the microchannel device was observed. The outlet temperature was evidently lesser than the inlet temperature due to the thermal gradient boundary condition of 200C. This can be attributed to the lack of insulation on the platen assembly during the bonding cycle, which propagated heat loss. To have a comparison with a device with no thermal stresses, a thermal profile was generated

without any thermal gradient boundary condition. The boundary condition of convective heat transfer mechanism in the microchannel device was also removed. This was done to view the effects of a uniform temperature throughout the stack on the microchannel device. The inlet and outlet temperatures were set to 1000C and a model was generated.

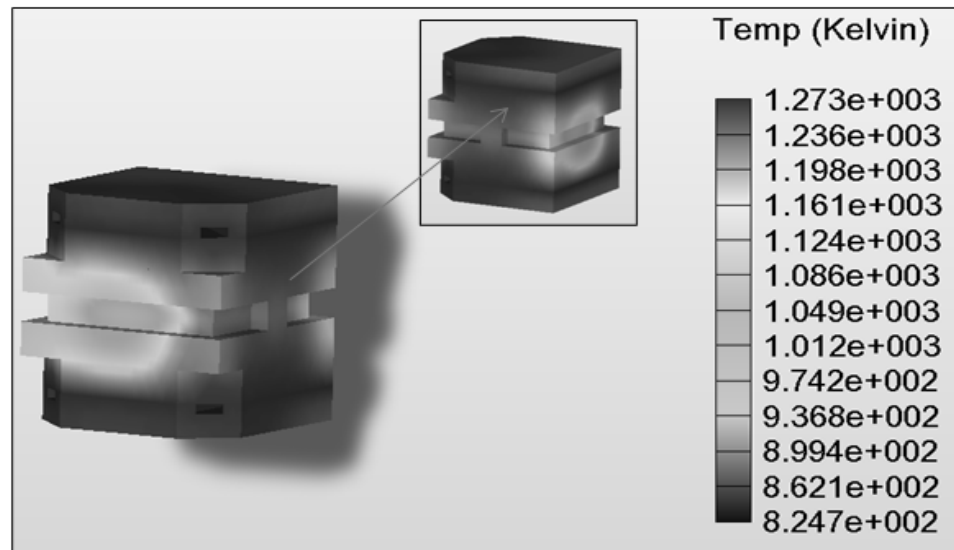


Figure B6. Thermal stresses on the stack without any gradients

Figure B6 shows the thermal stresses on the stack without any thermal gradients. The top and bottom platens were observed to be at 1200 K quite consistently. However, certain regions of the device were around the 1000K-1100K temperature zones. Although it is not a very large difference but it may impact the bond structures in the microchannel device as their dimensions are significantly smaller. The temperature profile of this device was not very different from the one which was exposed to non uniform heat (fig B5). However, the rear part of the stack showed a different heat pattern to that at the front. The difference was that the front front and back back regions were heated a lot lesser than the rest of the stack. This could be attributed to the channel geometry on the

platens which assist more volumes of gas in the certain regions which thereby undergo significantly large heating.

This model was able to validate that the microchannel device could be heated to the bonding temperature with the current stack design and geometry which implies that the internal convective heat from the argon gas could successfully diffusion bond highly parallel microchannel arrays. The next step was to develop a mechanism to supply the heat to this platen assembly. An inconel heat exchanger was fabricated to do this job.

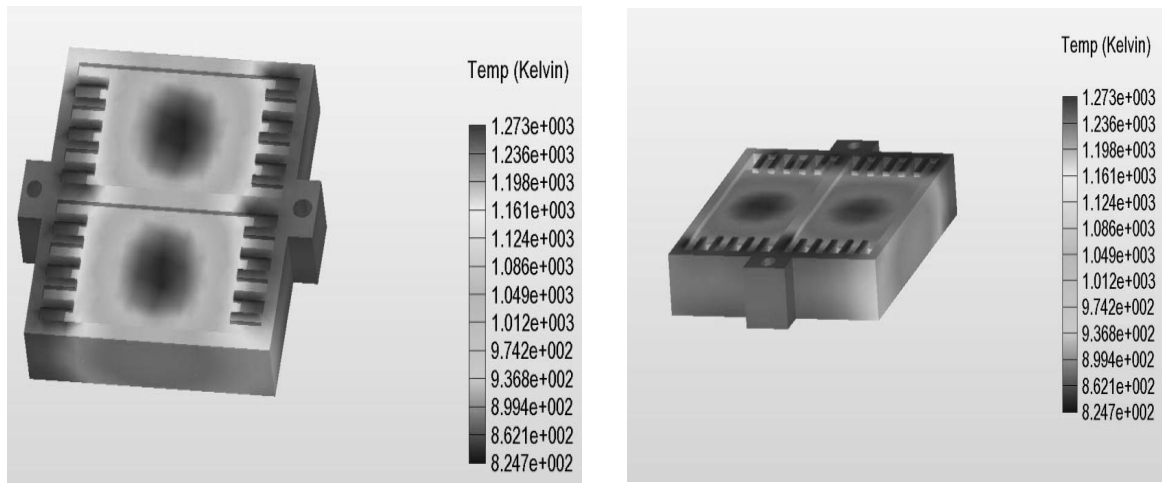


Figure B7 . Thermal profile on the microchannel device

Heat Exchanger Modeling

The material used for the inlet heat exchanger is Inconel (INC) 625 which is an excellent general purpose material for high strength applications at elevated temperatures

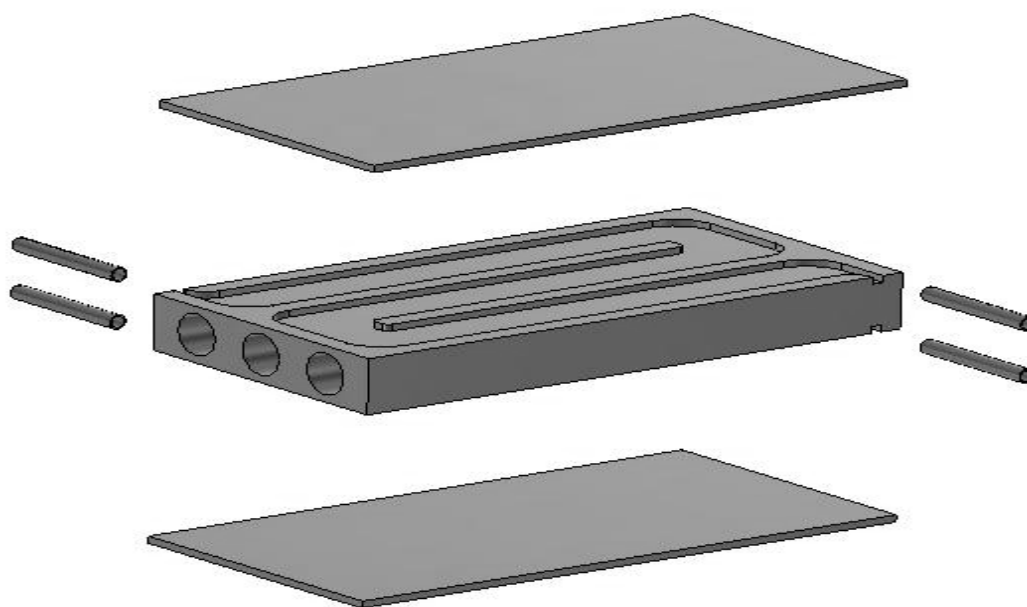


Figure B8. Exploded view of INC 625 Heat Exchanger

in oxygen atmospheres. An exploded view of the heat exchanger is shown in Figure B8. As shown in the figure, the INC 625 heat exchanger at the inlet consists of a centre block, a top and a bottom plate and some additional Inconel tubing. The centre block has dimensions of 8.5"x4.5"x1.0". Channels are machined on either side of the centre block to allow for the passage of argon gas from two inlets to two outlets. In the middle of the block are three 0.75" diameter through holes for placing nichrome heaters. The heaters are each capable of transferring up to 1000 watts of thermal power at 1400K.

The channels on the centre block are covered at the top and bottom by two INC 625 plates (8.5"x4.5"x0.125"). The two inlets and two outlets of the heat exchanger are connected to tube fittings. An estimate of the thermal requirements for the ICH system can be made by considering the enthalpy of the thermal mass in the system and making assumptions about heat losses. In our model, we are assuming that heat transfer to the gas

occurs from only one wall. This wall is held at a constant temperature of 1200K. The constant temperature boundary condition is present when the duct has a constant wall temperature in both the circumferential and the axial directions.

$$u = Q / A;$$

Where,

Q is the volumetric flow rate and

A is the cross sectional area of channel

$$u = 0.000416 \text{ m}^3/\text{sec} / 0.0000772 \text{ m}^2$$

$$= 5.388 \text{ m/sec}$$

The thermodynamic properties of argon gas were calculated at different temperatures ranging from 298-1200K. The values of molecular weight, density, specific heat, viscosity and thermal conductivity of argon at 298, 748, and 1200K are provided in Table 2. In order to design a plate-type heat exchanger capable of meeting these requirements, the mass flow rate and an estimation of the convective heat transfer coefficient is needed.

Coefficient of heat transfer and mass flow rate calculations

The convective heat transfer coefficient for this application can be estimated by,

$$h = Nu_T \cdot k / D_h \quad (2)$$

Where,

Nu_T ~ Nusselt number at constant wall temperature of 925 °C

D_h ~ hydraulic diameter

k ~ thermal conductivity of argon

h ~ coefficient of heat transfer

Nusselt number for fully developed laminar flow in rectangular ducts with heat transfer through one wall is 0.5322 [28].

Table B2. Thermodynamic properties of argon			
Temperature, K	298	748	1200
Molecular weight (MW), kg/mol	0.039	0.039	0.039
Density (ρ), kg/m ³	1.633	1.024	0.526
Specific heat (C_p), kJ/kg.K	0.520	0.520	0.520
Viscosity (η), kg/m.sec (10 ⁻⁵)	2.26	4.44	5.99
Thermal conductivity (k), W/m.K	0.01769	0.0351	0.048

The hydraulic diameter is given by,

$$D_h = 4ab / (2(a+b)) \quad (3)$$

Where,

a and b are channel height and width respectively

$$D_h = 0.00543\text{m}$$

The mass flow rate can be calculated as: $m = \rho \cdot Q$

(4)

Where,

$\rho \sim$ density of argon gas

$Q \sim$ volumetric flow rate

The volumetric flow rate for heating incoming argon gas to 1200K according to model developed previously is 25lt/min. Hence, this will be the volumetric flow rate at which the room temperature argon must enter the Inc 625 heat exchanger.

$$25 \text{ lt/min} = 0.000416 \text{ m}^3/\text{sec}$$

The coefficient of heat transfer and mass flow rate was calculated using the equations mentioned earlier and the values obtained are shown in table B3.

Table B3. Coefficient of heat transfer and mass flow rate			
Temperature(K)	298	748	1200
Heat Transfer Coefficient (W /m ² K)	1.832	3.370	4.702
Mass flow rate(kg/sec)	0.00067	0.00042	.00021

Calculation of Reynolds number

In fluid mechanics, the Reynolds number is the ratio of inertial forces to viscous forces and consequently it quantifies the relative importance of these two types of forces for given flow conditions. Thus, it is used to

identify different flow regimes, such as laminar or turbulent flow.

$$Re = (u \cdot D_h) / \nu$$

Where, u is the velocity of the gas; ν is the kinematic fluid viscosity

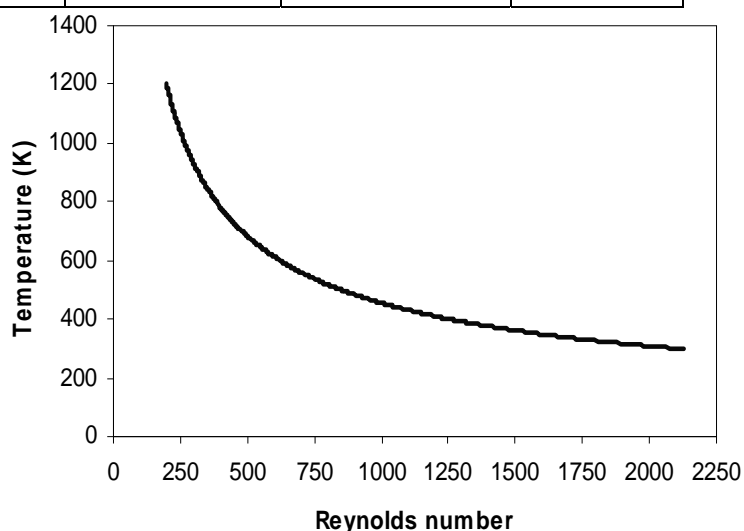


Figure B9 .Variation of Reynolds number with temperature

$\nu = \eta / \rho$ where, η , ρ are viscosity and density of argon gas respectively

Also,

$u = Q / A$ where,

Q is the volumetric flow rate and

A is the cross sectional area of channel machined in the heat exchanger.

$$u = 0.000416(\text{m}^3/\text{sec})/0.0000772 \text{ m}^2 = 5.388 \text{ m/sec}$$

The plot of Reynolds number against the temperature is shown in fig.B9. The values of Reynolds number suggests laminar flow at high temperatures. A Reynolds number greater than 2300 lies in the turbulent flow region. In our case, this around the 400-600 range.

Thermal model of heat exchanger

A thermal model based on the parameters of argon gas, heat transfer coefficient, and the channel dimensions of the heat exchanger was generated. The purpose of the thermal model was to determine if the surface area of the channel would be sufficient to heat the argon gas coming in at room temperature to the bonding temperature of the device. Figure B10 shows the distance traveled by the gas in the channel of the heat exchanger before it gets heated to the bonding temperature of the stack which is roughly 1200K. The results showed that the argon gas was heated to greater 1150K within a distance equal to approximately twice the channel height (6 mm from inlet). The heat distribution proves that the channel area provided in the heat exchanger would be sufficient for raising the gas temperature to 1200K from room temperature.

Heated fluid (inert gas, reducing gas, or other) can be forced through the prepared shim stack to provide the heat of bonding. This internal convective heating, or “furnace-less bonding,” technique can provide the assembly with rapid heat input while

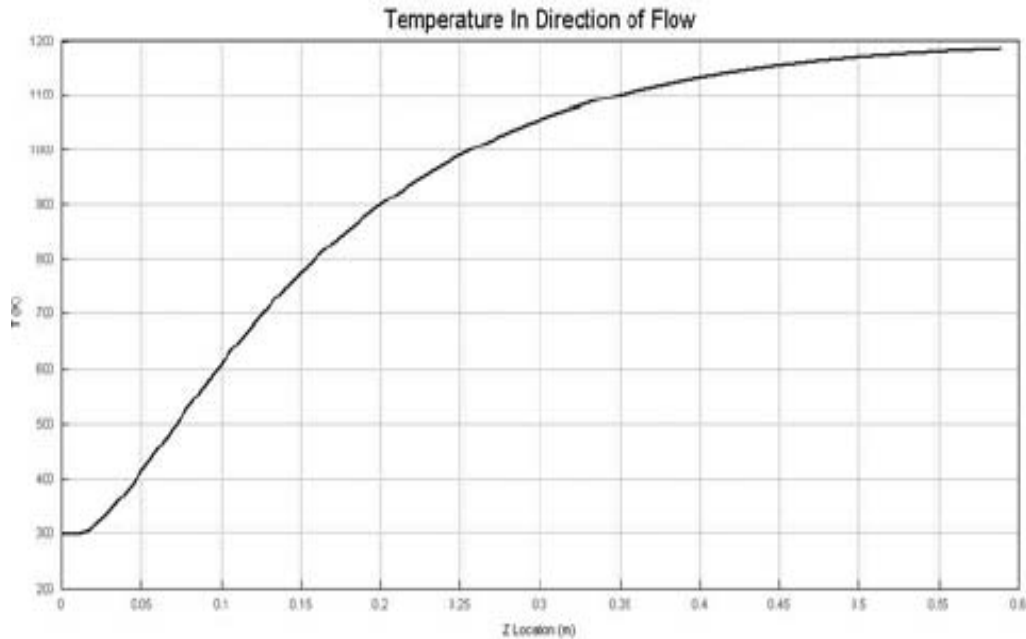


Figure B10. Temperature profile of the gas flow in the heat exchanger

minimizing thermal gradients within the assembly. Argon at 1200K was used to raise the temperature of the platen assembly to the diffusion bonding temperature.

Figure B11 shows the temperature distribution of argon flowing into the inlet and through a small length of channel, which was machined on the centre plate of the heat exchanger. The inlet velocity was set to the calculated value and the temperature of the incoming Argon gas was set to 298K. Argon gas properties were provided in piece-wise linear form using data for temperatures 298K, 748K and 1200K. The top wall boundary was set to 1223K, while all other walls were defined as adiabatic, or completely insulated.

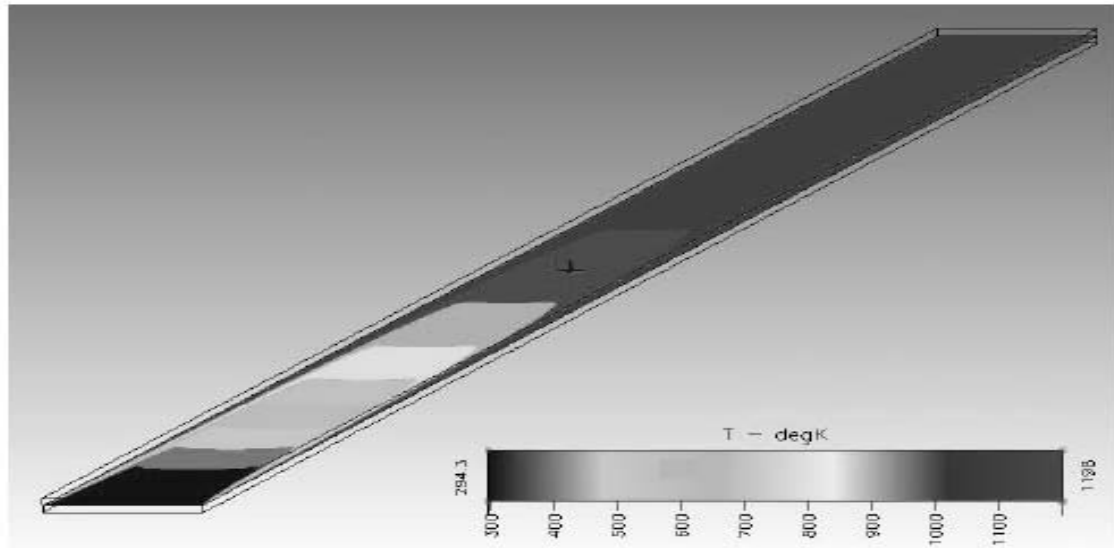


Figure B11. The temperature profile of Argon gas in the channel

The thermal distribution parallel to the channel length shows a gradual change in temperature from the inlet towards the outlet of the heat exchanger channel. The distribution parallel to the inlet plane shows the uniformity of the temperature distribution within the channel at certain point of time. The Argon gas was heated to greater 1150K within a distance equal to approximately twice the channel height (6 mm from inlet). The heat distribution proved that the channel area provided in the inlet heat exchanger would be sufficient for raising the gas temperature to 1200K from room temperature. We could now go ahead fabricate the heat exchanger.

LEAKAGE STUDY ON PLATEN ASSEMBLY

The objective of the leakage study was to investigate the amount of gas leakage resulting from an ICH setup.

Table B4. Leakage test variables	
Independent variables	Dependent Variables
Gas flow rate, Clamping pressure, Surface conditions: flatness, roughness, burr height	Volumetric Leakage

The leakage between the laminae and platens was studied as a function of applied pressure to the stack and surface conditions of the laminae. Leakage tests were performed to determine the clamping pressure required to acceptably minimize leakage of

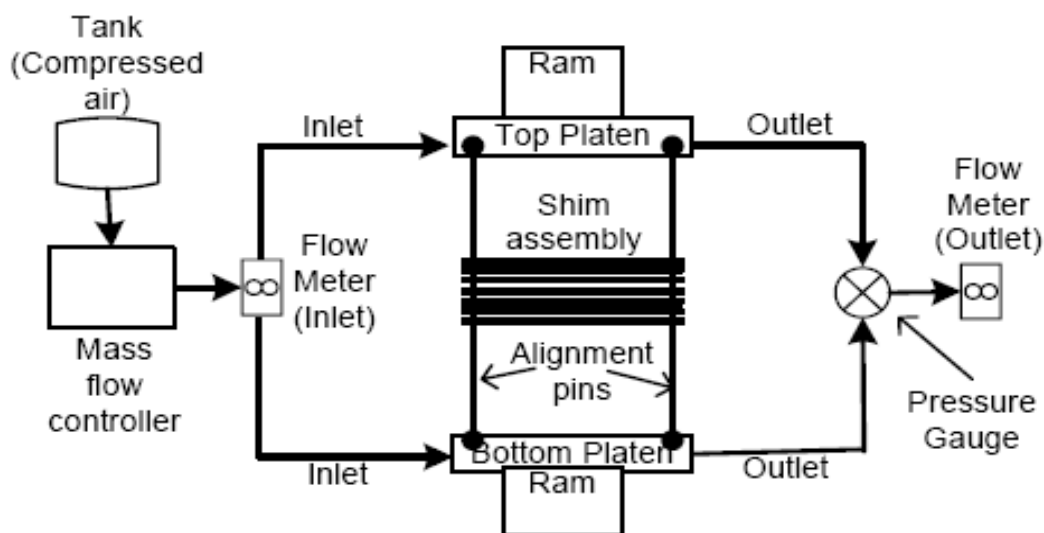


Figure B12. Conceptual design of leakage tests

convective gases from the bonding assembly. It was hoped that clamping pressures would be on the same order of magnitude as bonding pressure or lower. The temperature of the gas in the assembly will be near or at 1000C, which is the required temperature for the diffusion bonding of stainless steel. Thus the minimization of leakage is also critical to maximize safety. Process conditions to be investigated by the study are shown in Table

B4. The platens consist of an inlet and an outlet slot allowing for the entry and exit of argon gas. Stainless steel tubing was TIG welded onto the inlet and outlet slots of each platen. Holes were machined on the platens for pin alignment of the laminated shims.

LEAKAGE TEST SETUP

Figure B12 shows the shim assembly stacked in between the two platens, ready to be leak tested. A mass flow controller and a flow meter were connected to the inlet of the compressed air loop at close proximity to the vacuum hot press. A flow meter and a pressure gauge were connected to the outlet stream of the platen assembly. The purpose of the pressure gauge was to measure and vary the back pressure at the outlet of the flow loop. Finally, the assembly was clamped between the hydraulic rams of the vacuum hot press. As a preliminary leak test, the platens were clamped together with a 'C-clamp'. The assembly was immersed in a beaker containing water, and pressure was applied to check for bubbles. There was no bubble formation within the platens up to a pressure of 35 psi, indicating no leakage from the part. Before stacking, the shims were cleaned in a solution of Citranox and water. Grease was removed by acetone followed by ethanol and de-ionized water for removal of residues. The set of cleaned laminae were then assembled and aligned with the slots provided on the bonded platen assembly using 1/16" diameter alignment pins. For our final tests, the platen assembly was clamped between the rams of the vacuum hot press and the pressure was kept at a minimum level. The compressed air was turned on and passed through the platen assembly. The clamping pressure was gradually increased using the pressure control panel on the vacuum hot press. Volumetric flow rates at the outlet were measured with increasing clamping pressure using the flow meter provided at the outlet shown in Figure B12.

APPENDIX C

RESULTS AND DATA COLLECTION

Devices bonded on the vacuum hot press were compared with those made using the internal convective heating process. Metallographic sample preparation was used to find the true structure of the sample. Metallographic specimens were mounted using thermosetting resin and hardener mix. Thermosetting resins have been used in the past, but modern epoxy is becoming more popular because reduced shrinkage during curing results in a better mount with superior edge retention. After mounting, the specimen were cut open using a diamond saw and polished to reveal the surface of the metal. The specimen was successively ground with finer and finer abrasive sand paper. The ratings were used from 180, 320, up to 600 grit. Metallographic metrics of warpage and void fractions were used for data analysis and comparison. A brief description of methods to calculate these are given below.

Warpage Calculations

Warpage is a distortion where the surfaces of the bonded part do not follow the intended shape of the design. Warpage results from thermal stresses, which, in turn, is caused by differential heating of material in the molded part.

Warpage is measured using the following relation,

$$W = \Delta X / l$$

Where,

ΔX is the channel deviation or deformation that has occurred and l is the length over which that deformation has occurred.

Simply, warpage can be defined as the percentage deformation over a particular length of the channel.

Void Fraction Calculations

Void fractions can be defined as the ratio of the volume taken up by air spaces (the voids) to the total volume of a material. Clearly, void fractions need to be at the minimum in any microchannel device. This is because they can become a cause for leakage and also reduce the bond strength of the device. Usually, microchannel devices with less than 2% void fractions are considered acceptable. In some cases, grain boundaries can be mistaken for void fractions. This will be resolved by performing an aqua regia test on the region under study.

Creep Phenomenon

Under constant low-stress loading, and over extended time periods, many materials undergo creep, a permanent deformation that is particularly marked at elevated temperatures. Creep is defined as the tendency of a solid material to deform permanently under the influence of stresses at high temperatures. It usually occurs as a result of long term exposure to levels of stress that are below the yield strength or ultimate strength of the material. Creep is more severe in materials that are subjected to heat for long periods, and near the melting point.

Creep is a performance-based behaviour since it is not an intrinsic materials response. Furthermore, creep is highly dependent on environment including temperature and ambient conditions. Creep can be defined as time-dependent deformation at absolute

temperatures greater than one half the absolute melting. Creep is a relative phenomenon which may occur at temperatures not normally considered high.

Since all mechanisms of steady-state creep are in some way dependent on diffusion, we expect that creep rate will have this exponential dependence on temperature. Creep occurs faster at higher temperatures. However, what constitutes a high temperature is different for different metals.

Figures C1 and C2 show the metallographic examination of SS 316 shims bonded at 1000 C and 950 C showed the creep damage distribution caused by the multiaxial stresses in SS316 microchannels. This finding may have application in the design, life prediction, and in-service evaluation of diffusion bonded stainless steel microchannel devices. More figures in the appendix show the creep phenomenon caused due to stresses at high temperatures.

Difference between Creep and Warpage

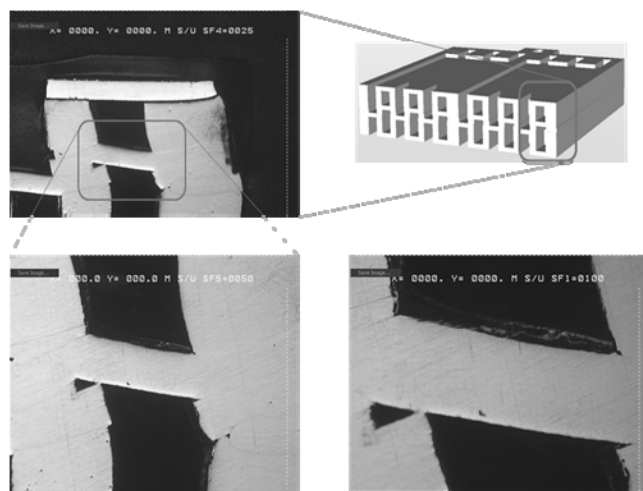


Figure C1. Creep mechanisms

The creep phenomenon must not be mistaken for deformation caused due to

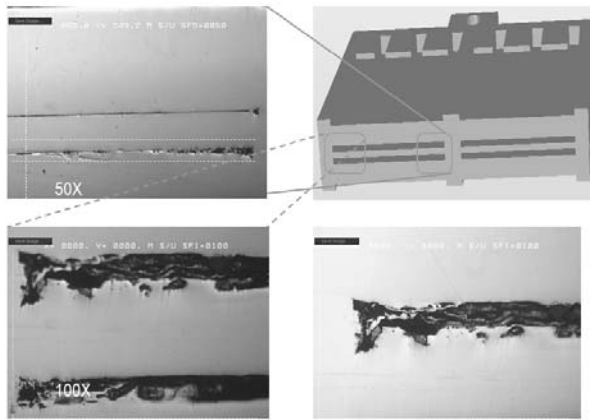


Figure C2a. Channel micrograph at 1000 C

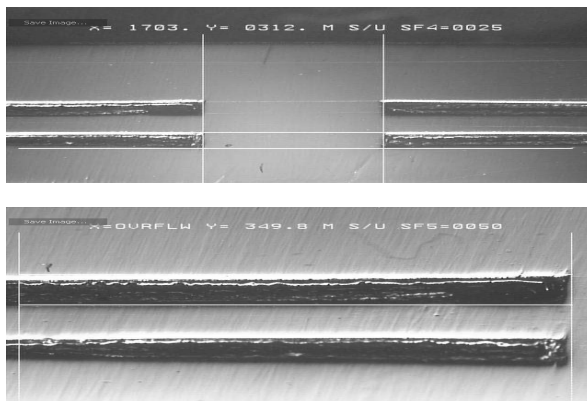


Figure C2b . Channel micrograph at 950 C

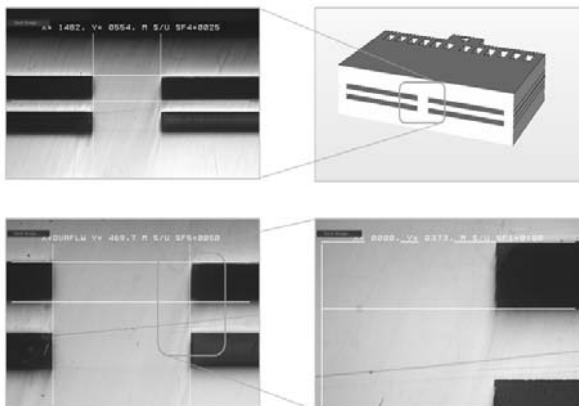


Figure C2c. Channel micrograph at 900 C

thermal stresses. Creep is a time and temperature phenomenon, whereas ‘warpage’ occurs due to thermal gradients due to differential heating in the device being bonded at high temperatures. This will be clearly understood by observing the results obtained at lower temperatures using the ICH and VHP process, the VHP devices having significantly deformed as compared to the ones fabricated using ICH.

Several sources have been identified for causing warpage within microchannel arrays. One source of microchannel warpage can be

the application of bonding pressure on regions of external laminae adjacent to microchannel regions. Another noted source of warpage can come directly from warpage in the raw shimstock, foil or film [MECS chapter].

Perhaps the greatest source of warpage can come from sideloads on the foils either due to friction between laminae, friction between external laminae and the fixture or due to the registration technique. Slower temperature ramps in the bonding cycles can help ameliorate some of these causes of warpage.

Final conditions for comparison of test coupons

The biggest challenge was to find a set of conditions which could clearly compare and contrast the VHP and ICH processes. This was accentuated further by the occurrence of the creep phenomena at around 1000C. Samples were bonded at 900, 950 and 1000 C to determine the temperature around which creep disappears. The results showed that at temperatures above 900 C, creep started happening in stainless steel 316 shims. This has already been shown in figure C2. The devices were being bonded at a pressure of 3500 psi. From this analysis, we were able to conclude that the final bonding conditions needed to be at 3500 psi and 900 C. A low ramp rate of 8^0 C/ min was being used for all these experiments.

We have learnt from past experiences that this is the maximum ramp rate the VHP is capable of supplying. However, one import thing to note here is that all these tests were performed without the addition of helium during the cooling cycle. The significance of this will be explained in a latter section.

Internal Convective Heating bonding Cycle – Preliminary Experiments

The main objective of this experiment was to identify a set of bonding conditions which would contrast the internal convective heating (ICH) process with bonding processes on the vacuum hot press (VHP). The Bonding Conditions used for the experiment were:

- Temperature - 900⁰ C
- Pressure - 3500 psi
- Bonding time - 2 hours
- Ramp up rate – 20⁰ C/min
- Ramp down rate – 20⁰ C/min

The ICH is capable of providing ramp rates of over 50 C/ min. However, for the sake of comparison, the conditions were the same as those used while diffusion bonding samples on the VHP.

Results and Conclusions from Preliminary run

Some of the key outcomes from this run are as follows. There were some sections which had not bonded and had a lot of leakage through them. This could have either been a parallelism issue or because of inadequate thermal conditions in the ICH process. Leakage was determined by performing pressure tests on the devices. Void fractions were mainly due to the lack of parallelism in the insulation blocks for the 1st ICH run. This was resolved later by using highly parallel zirconia blocks above and below the bondin

assembly. Results of that will be shown later. ICH sample showed minimal warpage due to thermal gradients.

Table C1. ICH Thermocouple data from run 1

Bonding time (mins)	T1 (top inlet temp)	T2(bottom inlet temp)	T3(Top outlet temp)	T4(bottom outlet temp)	Heat Ex Temp	Pressure(transducer)	Gas flow rate (lt/min)
7	885	830	660	633	1000	28.44	21.715
20	940	879	691	660	1071	28.81	21.708
30	958	895	721	688	1087	28.9	21.722
40	Melted	891	726	693	1087	28.9	21.713
60	melted	melted	729	695	1087	28.9	21.717
70	Melted	melted	729	695	1087	28.9	21.717
90	Melted	melted	729	695	1087	28.9	21.717
110	Melted	melted	727	693	1087	28.9	21.717

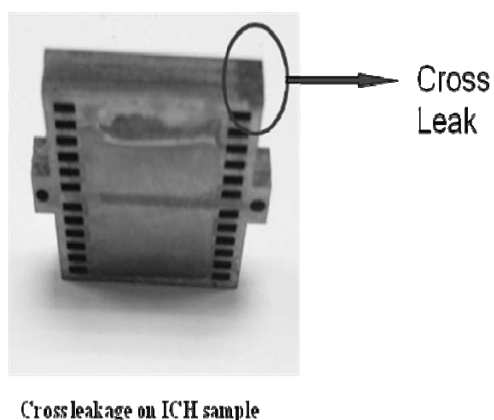
Also, it was also observed that two of the thermocouples had melted. This was because of lack of proper insulation which caused overheating of wires placed close to the heat exchanger. However, the positives that came out of the run were that ICH is able to handle high pressures. Also, the micrographs proved that the geometry of the channels

was acceptable in terms of standards for microchannel devices (Figure C6). We had to now take care of the parallelism issue and the thermal insulation problem.

Pressure tests

The test article was clamped to a pressure testing device using miniature clamps. All tests were performed at room temperature and atmospheric pressure. A flow path was created by cutting out a channel on silicone having the same dimensions of the test article. The system was pressurized using a hand pump. Snoop fluid was applied to check for leakage in suspected areas.

The devices were checked for internal and external leaks. A pressure of 25psig was applied to the system. The circled regions show bubbles in the figure at the regions of maximum leakage. It was observed that the loss of pressure in the system was



Pressure tests on ICH sample #1 using a hand pump

Figure C3. Pressure test results

negligible over 5 minutes. The first ICH sample showed cross leaks as well as external leaks. The devices bonded using the vacuum hot press showed no signs of leakage. The regions showing leakage on the ICH sample were investigated using metallography to identify reasons for leakage. At this stage, our next steps were to fix the problems that occurred in the first run and look for the set of conditions that would provide a comparison between the ICH and the VHP process. However, there was a problem that occurred with the heat exchanger that needed to be fixed at first.

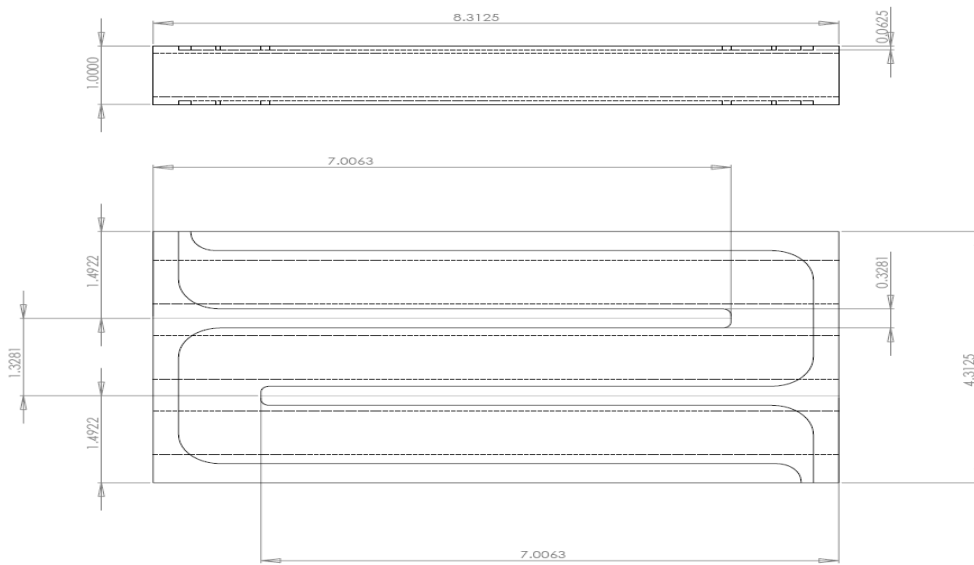


Figure C4. Heat exchanger remachining specifications

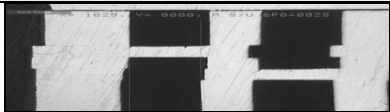







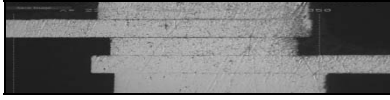
Heat Exchanger Deformation




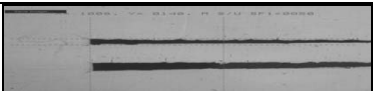
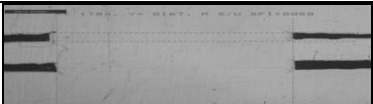
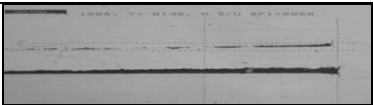
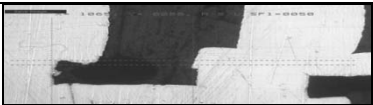
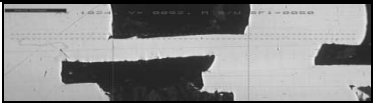
A bulge occurred on the top and bottom surface of the heat exchanger due to heat expansion at the time of bonding cycle. The top/bottom plates were welded on to the centre block. Since the plates were not bonded to the channels, they expanded. A simple mill/weld combination was performed to fix this problem.

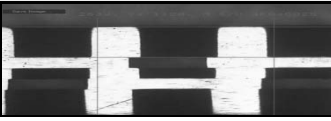

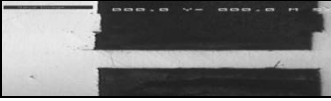

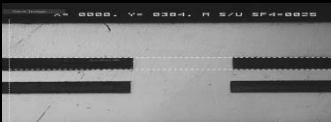
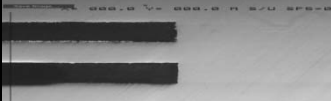
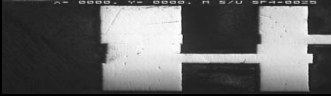
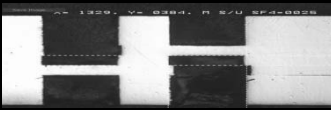
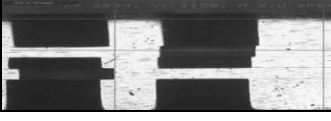
A 1/8" deep cut was made through the top/bottom plates back above the ribbed section of the heat exchanger and welded through the surface of the cut to make sure there was a permanent bond between the plates and the channel block. Further runs could then be ensured on the ICH system. Detailed diagrams of the remachining process are given in the appendix.

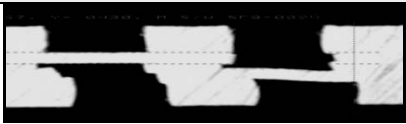
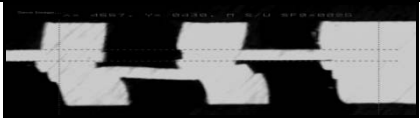

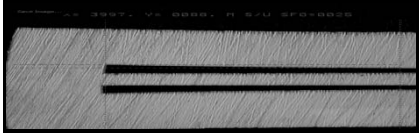
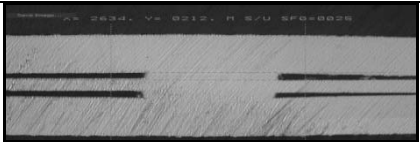
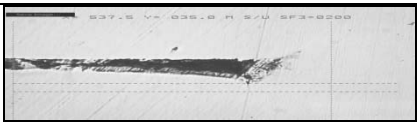
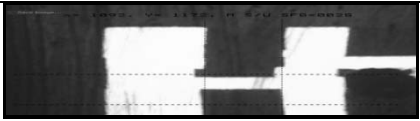
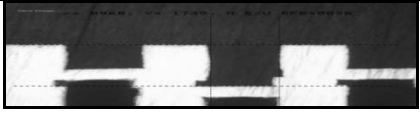

Warpage and Void Fraction results based on final conditions for ICH and VHP samples.

Table C2, C3, C4 and C5

Device	Cross Section	Micrograph	Span (μm), Mag	Void Fractions	% Warpage
ICH 1	Inlet (front)		1000, 25x	1.84	1.5
ICH 1	Inlet (Centre)		500, 50x	1.26	0.19
ICH 1	Inlet (Back)		500, 50x	2.72	Nil
ICH 1	Channel (front)		1000, 25x	1.37	0.67
ICH 1	Channel (centre)		1000, 25x	2.19	Nil
ICH 1	Channel (back)		1000, 25x	2.7	Nil
ICH 1	Outlet (front)		500, 25x	1.9	1.2
ICH 1	Outlet (centre)		500, 50x	2.39	1.4
ICH 1	Outlet (back)		500, 50x	4.6	Nil

Device	Cross Section	Micrograph	Span (μm), Mag	Void Fractions	% Warpage
VHP 1	Inlet (front)		500, 50x	Nil	59/1000= 5.9%
VHP 1	Inlet (Centre)		1000, 25x	Nil	74/1000= 7.4%
VHP 1	Inlet (Back)		1000, 25x	0.36	160/1137= 14.07%
VHP 1	Channel (front)		1000, 50x	Nil	140/1000= 14%
VHP 1	Channel (centre)		1000, 50x	0.43	157/1110= 14.7%
VHP 1	Channel (back)		1000, 50x	Nil	145/1000= 14.5%
VHP 1	Outlet (front)		1000, 50x	Nil	88/1065= 8.2%
VHP 1	Outlet (centre)		1000, 50x	Nil	92/1024= 8.9%

Device	Cross Section	Micrograph	Span (μm), Mag	Void Fractions	%Warpage
ICH 2	Inlet (front)		1000, 25x	0.38	15/1000= 1.5%
ICH 2	Inlet (Centre)		500, 50x	0.36	24/1000= 2.4%
ICH 2	Inlet (Back)		1000, 50x	0.95	Nil
ICH 2	Channel 1 (front)		1000, 50x	1.47	Nil
ICH 2	Channel 1 (centre)		1000, 25x	1.34	Nil
ICH 2	Channel 1 (back)		500, 50x	1.78	Nil
ICH 2	Outlet (front)		500, 25x	1.67	Nil
ICH 2	Outlet (centre)		500, 25x	1.8	Nil
ICH 2	Outlet (back)		1000, 25x	3.2	32/1000= 3.2%

Device	Cross Section	Micrograph	Span (μm), Mag	Void Fractions	% Warpage
VHP2	Inlet (front)		1000, 25x	Nil	79/1000= 7.9%
VHP2	Inlet (Centre)		1000, 25x	Nil	82/1000= 8.2%
VHP2	Inlet (Back)		1000, 25x	Nil	94/1000= 9.4%
VHP2	Channel (front)		1000, 25x	Nil	65/1000= 6.5%
VHP2	Channel (centre)		1000, 25x	Nil	78/1000= 7.8%
VHP2	Channel (back)		1000, 200x	Nil	161/1000= 16.1%
VHP2	Outlet (front)		1000, 25x	Nil	73/ 1000= 7.3%
VHP2	Outlet (centre)		1000, 25x	Nil	81/1000= 8.1%
VHP2	Outlet (back)		1000, 25x	Nil	89/1000= 8.9%

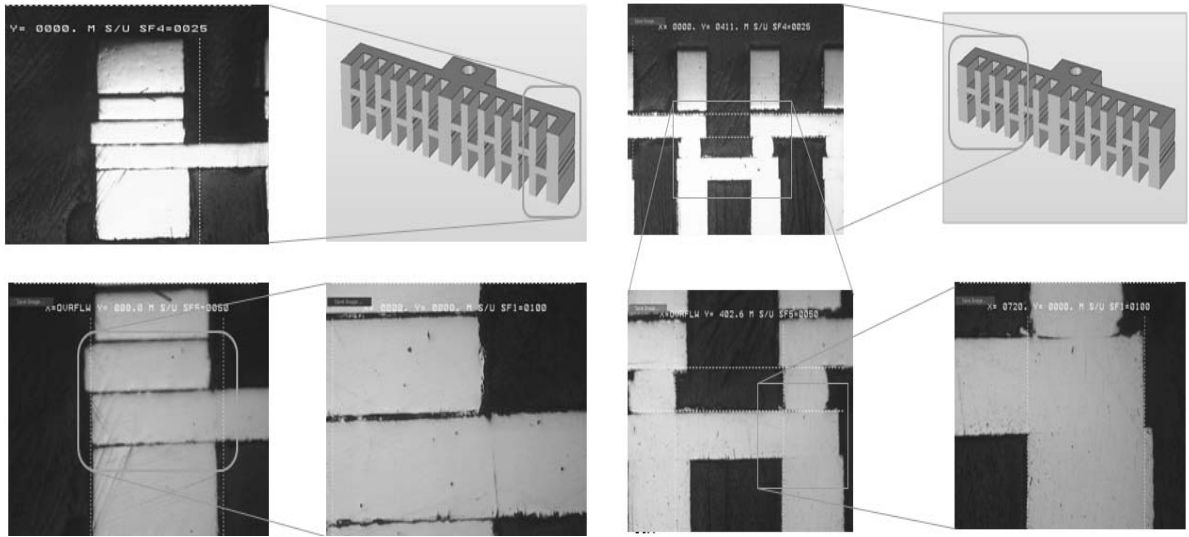


Fig C5. Unbonded regions due to bad parallelism in ICH run 1

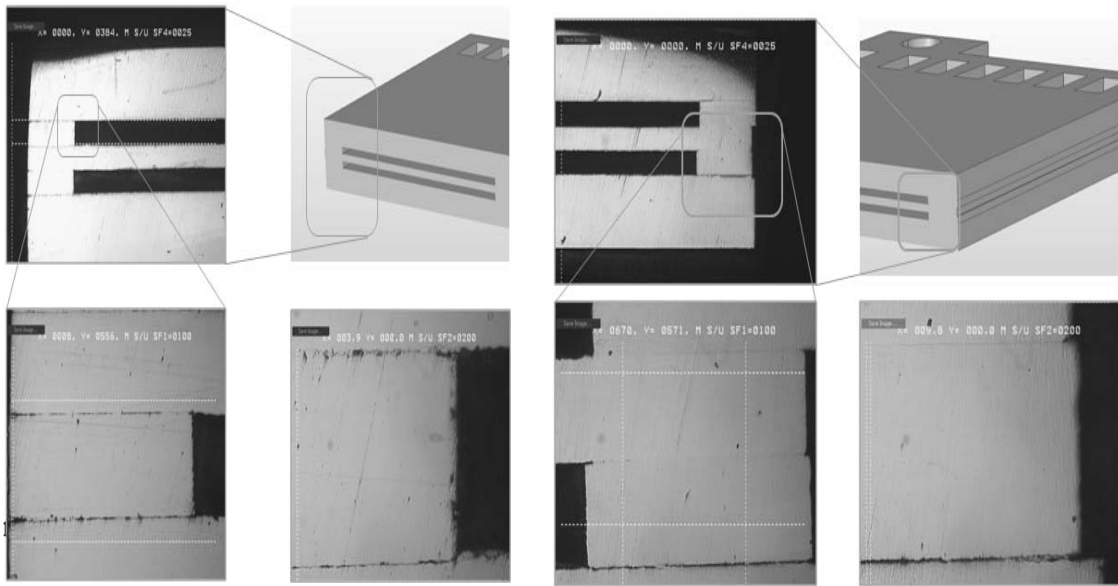


Figure C6. Good channel geometry in first ICH device

Results from mean void fraction and warpage calculations for ICH sample 1 and VHP sample 1 are shown in the tables C6, C7 and C8. The warpage in the VHP samples is significantly greater than the warpage in ICH samples. This is due to the thermal stresses caused by high cooling rates in the hot press.

Table C6 : Void Fraction and warpage at the inlet

Section	ICH 1		VHP 1	
	Voids (%)	Warpage (%)	Voids (%)	Warpage (%)
Inlet (front 1)	1.84	1.5	0	5.9
Inlet (front2)	1.75	2.4	0	6.8
Inlet (middle 1)	1.86	0.19	0	7.4
Inlet (middle 2)	1.91	0.54	0	5.4
Inlet (back 1)	2.72	0	0.36	14.07
Inlet (back 2)	2.79	0	0.45	15.3
Mean	2.145	0.771666667	0.135	9.145

Table C7 : Void Fraction and warpage at the outlet

Section	ICH 1		VHP 1	
	Voids (%)	Warpage (%)	Voids (%)	Warpage (%)
Outlet (front 1)	1.9	1.2	0	8.2
Outlet (front 2)	2.72	0.39	0	7.6
Outlet (middle 1)	2.39	1.4	0	8.9
Outlet (middle 2)	2.17	0.43	0	17.8
Outlet (back 1)	3.6	0	0.49	15.8
Outlet (back 2)	4.3	0	0.32	16.9
Mean	2.846666667	0.57	0.135	12.53333333

Table C8 : Void Fraction and warpage at the channel

Channel (front 1)	1.37	0.67	0	14
Channel (front 2)	1.45	0.72	0	14.2
Channel (middle 1)	2.19	0	0	14.7
Channel (middle 2)	2.65	1.3	0	15
Channel (back 1)	2.7	0	0	14.5
Channel (back 2)	2.9	1.5	0	13.6
Mean	2.21	0.698333333	0	14.33333333

Bibliography

Chapter 2

¹ Kearns, W.H., 1980, Welding Handbook: Resistance and solid state welding and other joining processes, 7th Edition, volume 3, American welding society, Miami, florida, USA.

² B. K. Paul, R. B. Peterson, "Microlamination for Microtechnology-based Energy, Chemical, and Biological Systems," ASME International Mechanical Engineering Congress and Exposition, Nashville, Tennessee, AES Volume 39, November 15-20, (1999), pp. 45-52.

³ H. Loewe, W. Ehrfeld "State-of-the-Art in Microreaction Technology: Concepts, Manufacturing and Applications", *Electrochimica Acta*, (1998), vol. 44, pp. 3679-3689.

⁴ K. P. Kaemper, W. Ehrfeld, J. Doepper, V. Hessel, H. Lehr, H. Loewe, h.Richter, A. Wolf, "Microfluidic Components for Biological and Chemical Microreactors", *Proceedings IEEE Micro Electro Mechanical Systems*, (1997), pp. 338-343.

⁵ Paul, B.K., P. Kwon, R. Subramanian, "Understanding limits on fin aspect ratios in counterflow microchannel arrays produced by diffusion bonding," *J. Mfg Sci. Engr.*, 128(4): (2006), 977-983.

⁶ I. Beausoleil-Morrison, "The adaptive simulation of convective heat transfer at internal building surfaces," *Building Environment* 37 (2002), 791–806.

⁷ Peng XF, Peterson GP "The effect of thermo-fluid and geometric parameters on convection of liquid through rectangular microchannels," *Int J Heat Mass Transfer* 38(4): (1995), 755–758.

⁸ Warren M. Rohsenow, James P. Hartnett, Young I. Cho, *Handbook of heat transfer*, Tata McGraw Hill, Third Edition: Year, p.2.4-2.5, 5.67-5.72.

⁹ Paisarn Naphon "Laminar convective heat transfer and pressure drop in corrugated channels," *International Communications in Heat and Mass Transfer* 34 (2007), 62–71.

¹⁰ B. Sunden, S. Trollheden, "Periodic laminar flow and heat transfer in a corrugated two-dimensional channel," *International Communications in Heat and Mass Transfer* 16 (1989), 215–225.

Chapter 3

¹¹ U.S. Patent No. 6,129,261, 1996, "Diffusion bonding of metals" Sanders, Daniel G.

¹² P. M. Martin, D. W. Matson, A. L. Tonkovich, G. L. Roberts, "Fabrication of a Stainless Steel Microchannel Microcombustor Using a Lamination Process", *Proceedings of SPIE*, 1998, v. 3514, p. 386-392

¹³ P. M. Martin, D. W. Matson, W. D. Bennett, D. C. Steward, Y. Lin, *Laser Micromachined and Laminated Microfluidic Components for Miniaturized Thermal, Chemical and Biological Systems*, *Proceedings of SPIE*, 1999, v. 3680, p. 826-833

-
- ¹⁴ R. S. Wegeng, C. J. Call, M. K. Drost, "Chemical Systems Miniaturization," 1996 AIChE Spring Meeting, New Orleans, 1996
- ¹⁵ M. Martin, W. D. Bennett, and J. W. Johnson, "Microchannel Heat Exchangers for Advanced Climate Control," Proc. SPIE (v2639, 1996), pp. 82–88
- ¹⁶ G. Jovanovic, J. Zaworski, T. Plant, and B. Paul, Proc. 3rd Intl. Conf. on Microreaction Technology (Frankfurt, Germany), 1999.
- ¹⁷ B. K. Paul, T. Dewey, D. Alman, and R. D. Wilson, "Intermetallic Microlamination for High-Temperature Reactors," 4th Int. Conf. Microreaction Tech., Atlanta, GA, March 5–9, 2000, pp. 236–243.
- ¹⁸ B. K. Paul, and T. Terhaar, "Comparison of two passive microvalve designs for microlamination architectures," J Micromech. Microengr., (v10, 2000), pp. 15–20.
- ¹⁹ Kuan Chenn, Second-law analysis and optimization of microchannel flows subjected to different thermal boundary conditions, International Journal of energy research 2005; 29:249–263, 13 December 2004
- ²⁰ H. Loewe, W. Ehrfeld "State-of-the-Art in Microreaction Technology: Concepts, Manufacturing and Applications", Electrochimica Acta, 1998, v. 44, p. 3679-3689
- ²¹ S. B. Dunkerton (1991), "Diffusion bonding – process and applications", Welding and Metal Fabrication, v. 59, p. 132,134-136
- ²² I. Iswadi, H. Ogiyama, H. Tsukuda, "Solid State Diffusion Bonding of Superplastic Duplex Stainless Steel with Carbon Steel", Materials Science Research International, 2003, v. 9, p. 154-159
- ²³ Paul, B.K., P. Kwon and R. Subramanian, "Understanding Limits on Fin Aspect Ratios in Counterflow Microchannel Arrays Produced by Diffusion Bonding," *J. Mfg Sci. Engr*, 128(4): 977-983, 2006.
- ²⁴ Wattanutchariya, W. and B.K. Paul, "Bonding Fixture Tolerances for High-Volume Metal Microlamination Based on Fin Buckling and Laminae Misalignment Behavior," *J Intl Soc Prec Engr Nanotechnology*, 28(2): 117-128, 2004.
- ²⁵ Paul, B., D. Palo and S. Bose, "Internal Convective Heating for Metal Microchannel Bonding," International Conference on Micromanufacturing, Greenville, SC, 2007.
- ²⁶ C. Pluess and B. Paul, "Application of Controlled Thermal Expansion in Microlamination for the Economical Production of Bulk Microchannel Systems," *Chem Engr Comm*, 194(9): 2007, 1259 - 1270.
- ²⁷ Wattanutchariya, W. "Application of Buckling Behavior to Evaluate and Control Shape Variation in High-Temperature Microlamination," Ph.D. Dissertation, 2002.